ALADIN - HIRLAM NEWSLETTER

No. 2, April 2014

Flash floods on 7th June 2013, Melk Austria

HIRLAM-B Programme, c/o J. Onvlee, KNMI, P.O. Box 201, 3730 AE De Bilt, The Netherlands

ALADIN Programme, c/o P. Termonia, IRM, Avenue Circulaire 3, 1180 Bruxelles, Belgium

Contents

Introduction

Tilly Driesenaar and Patricia Pottier

We are happy to provide you with the second edition of the combined Newsletter of the HIRLAM and ALADIN consortium.
This edition contains of a number of contributions focussing on deeply convective events, and one on erroneously simulated fog at sea in Harmonie. Furthermore you can find national contributions describing main achievements at several meteorological institutes, as well as an extended summary of a PhD thesis by Vanja Blažica focussing on divergence in limited area models.

Finally a list of events that are planned for 2014 is added.

We hope you enjoy the second ALADIN-HIRLAM Newsletter!

For additional information please visit the ALADIN and HIRLAM websites, or just ask the authors.

http://www.cnrm.meteo.fr/aladin/

http://hirlam.org

Simulating downbursts with Alaro: a case study.

Pieter De Meutter, Luc Gerard, Geert Smet, Karim Hamid, Rafiq Hamdi, Daan Degrauwe and Piet Termonia

1 Introduction

On 18 August 2011, several convective cells developed over North-France and Belgium. One of these cells struck the Pukkelpop music festival in Kiewit (Belgium), at which about 60,000 people were present. The severe wind gusts at the festival, associated with a downburst, caused five casualties and injured more than 140 people.

In the frame of the Fujita project of the RMI, a damage survey has been made to estimate the wind gust speed at the Pukkelpop festival during the downburst. While many trees were uprooted, the damage on nearby residences was found to be marginal. Due to the fragmented nature and the pattern of damage, a tornado was found unlikely. The damage corresponded to the EF0 Enhanced Fujita scale (i.e. the lowest scale), with wind gusts ranging between 29 to 37 m s^{-1}. The downburst at the Pukkelpop festival had a width of less than 100 m and was accompanied by heavy precipitation and hail.

Unfortunately, it is very difficult to forecast severe convective storms like the one that struck the Pukkelpop music festival, since operational numerical weather prediction models (having grid spacings of a few kilometers) do not fully resolve convection (Weisman, 1997; Bryan, 2003). Our model uses a deep convective parameterization scheme to take into account the effects of subgrid convective processes, but these parameterizations have some degrees of freedom and need to be tuned.

Since the downdraft plays a crucial role in the creation of severe wind gusts, it is of great importance to correctly estimate the downdraft. Precipitation-cooled air in the downdraft sinks and forms a cold pool at the surface. Several precipitating thunderstorms can form a coherent cold pool with a horizontal diameter of the order of 100 km (Fujita, 1959; Johnson and Hamilton, 1988). The descending cold air causes a hydrostatic pressure increase at the surface, called a surface mesohigh, of which the strength depends on the temperature and depth of the cold pool (Wakimoto, 1982). Gusty winds in the cold pool originate from downward momentum transport and surface pressure perturbations (Vescio and Johnson, 1992). The difference in pressure can lead to a significant acceleration of air (Schmidt and Cotton, 1989).

Engerer et al. (2008) investigated the surface characteristics of cold pools from Mesoscale Convective Systems (MCS) using observations from the Oklahoma Mesonet. They found a mean temperature drop of 7 K and a pressure rise of 4.5 hPa for mature stage MCS. They suggest that if the model fails to represent cold pool characteristics correctly, improvements to the model physical parameterizations may be needed.

We have investigated the meteorological events of 18 August 2011 using radar observations, automatic weather station (AWS) data and numerical weather prediction (NWP) output. Particular attention is given to the downdraft, since most of the damage was caused by severe wind gusts associated with a downburst.

2 Data

Observations are obtained from automatic weather stations (AWS) over Belgium and a single-polarization C-band Doppler radar at Wideumont. Every ten minutes, the AWS provide measurements of 2m temperature, 2m dewpoint, station pressure and 10 min. accumulated precipitation. The simulations have been done using the limited area model ALARO (see e.g. De Troch et al., 2013).

2.1 ALARO model with unsaturated downdraft scheme

To take into account the subgrid effects of convection, the package 3MT (Modular Multiscale Microphysics and Transport) is used (Gerard et al., 2009). In our tests, the 3MT moist-downdraft scheme has been replaced by the parameterization of an unsaturated downdraft. The starting level for the downdraft is taken as the first minimum in the moist static energy below 500 hPa, since downdrafts start around the level of minimal equivalent potential temperature θ_e at approximately 650 hPa (Sud and Walker, 1993). The mean grid box wet bulb properties are taken as a starting point. Following the ideas of Betts and Silva Dias (1979), it is assumed that the downdraft follows a curve of constant θ_e, although remaining unsaturated. Moisture content is changed by entrainment and evaporation. The unresolved downdraft width is taken to be $1/3^{rd}$ of the precipitating area inside a grid box. A fixed entrainment rate is applied along the descent. It is parameterized by λ_d, a tunable parameter. A non-dimensional entrainment coefficient ξ is expressed as follows:

$$\xi'^{\overline{l-1}} = \lambda_d(\phi^{l-1} - \phi^l) \tag{1}$$

$$\psi_d^l = \psi_d^{l-1} + \xi'^{\overline{l-1}}(\psi_e^{l-1} - \psi_d^l) \tag{2}$$

$$\psi_d^l = \psi_d^{l-1} + \xi^{\overline{l-1}}(\psi_e^{l-1} - \psi_d^{l-1}) \qquad \text{with: } \xi = \frac{\xi'}{1+\xi'} \tag{3}$$

with ϕ^l the geopotential height of level l and ψ^l a physical variable at level l. The subscript d stands for downdraft, e for environment. The model levels are numbered from top to bottom, l stands for the center of the model layer l and $\bar{l}$ its lower interface, between l and $l+1$

The effect of drag and entrainment is represented in the vertical momentum equation as follows:

$$\frac{\partial \omega_d}{\partial t} = -\left((\lambda_d + K_{dd}/g)\,\frac{R_a T_{vd}}{\pi}\right)\omega_d^2 + \text{ other terms} \tag{4}$$

where the entrainment rate λ_d and the additional drag K_{dd} will be our main tuning parameters; g stands for the gravitational acceleration, π for the hydrostatic pressure, R_a for the dry air gas constant and T_{vd} is the downdraft virtual temperature. The other terms include buoyancy, vertical subgrid advection and a braking towards the surface (see Gerard, 2007). The unsaturated downdraft properties (and the buoyancy) result from the budget between the adiabatic warming and the evaporative cooling, so that an increased velocity reduces the saturation and further the negative buoyancy (and conversely), ensuring a negative feedback.

2.2 Different model runs

The Alaro model is used at 4 km resolution with the modified deep convective parameterization 3MT. The model has been used with default downdraft parameters (referred to as "BP40") and with new downdraft tunings based on the cold pool characteristics (referred to as "BP40-tuned"). These model runs have then been evaluated using observations and, since direct measurements of certain quantities such as downdraft speeds are missing,

a reference run at 1 km resolution (referred to as “BP10”) that is assumed to approach the behavior of fully resolved deep convection.

To asses the synoptic scale situation, we have used the operational ALARO model at 7 km resolution. From that, we found that the synoptic scale was characterized by a so-called Spanish Plume event (Carlson and Ludlam, 1968; van Delden, 1998).

3 Cold pool and mesohigh

Several AWS of the RMI show clear cold pools and associated mesohighs. Fig. 1 shows the observations of the AWS of Diepenbeek, the closest AWS to the Pukkelpop festival. A steady pressure drop is visible, which can be attributed to the approach of the thermal low, followed by a sharp pressure rise. The latter is accompanied by a steep decrease in temperature and the onset of precipitation. This pressure rise and temperature drop can be identified as the mesohigh and cold pool. The mean observed temperature drop was 6.4 K, while the mean pressure rise was 2.4 hPa (peak temperature drop of 7.4 K and peak pressure rise of 3.4 hPa). As noted by Engerer et al. (2008), the pressure perturbations are a better marker for the cold pool strength than the temperature drop, since the latter is sensitive to the diurnal cycle.

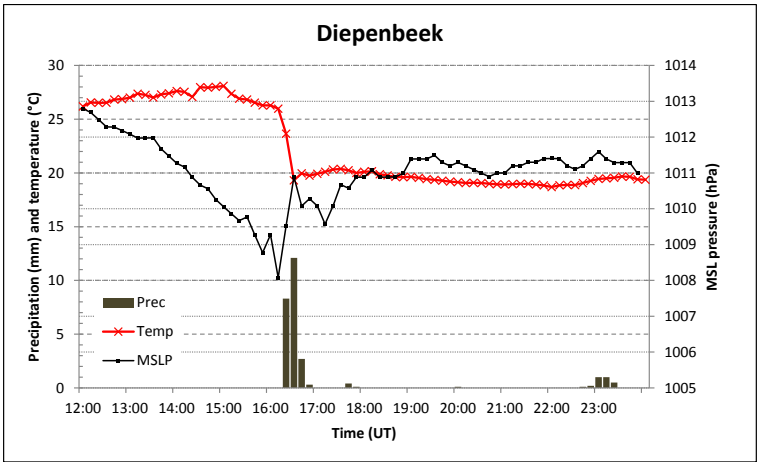

Figure 1: 10 min. observations of 2m temperature (°C, left vertical axis), MSL pressure (hPa, right vertical axis) and precipitation (mm, left vertical axis) from the AWS of Diepenbeek at 18 August 2011. The cold pool and mesohigh are cleary visible.

In the Alaro model, convective precipitation is accompanied by the formation of a cold pool with a local anomaly of about 4 to 5 K. The pressure in the thermal low becomes minimal near the updraft, while a surface mesohigh is visible inside the cold pool. The highest wind speeds are occurring at the boundary between the mesohigh and thermal low, were the pressure gradient is largest (peak wind gust of 17 m s^{-1}). A peak temperature drop of 5.7 K and peak pressure rise of 2.2 hPa were predicted.

4 Downburst predictability

4.1 Retuning the unsaturated downdraft scheme

By comparing the cold pool data from AWS and model forecast from BP40, we found that the cold pool predicted by BP40 is too weak compared to observations. In BP40, the cold air advection by the downdraft is too weak, since both the predicted temperature drop and the pressure perturbations are weaker than the observations indicate. Moreover, the dewpoint in the simulated cold pools becomes very high (up to 22°C), which is contrary to what the observations show and the reference run predict (both below 20°C).

Reducing the model downdraft entrainment and drag result in larger downdraft velocities and mass fluxes, while these remain realistic thanks to the negative feedback inherent to the unsaturated downdraft representation (as discussed in section 2). The stronger downdraft results in a stronger cold pool and mesohigh, as can be seen in Fig. 2. We tuned the unsaturated downdraft scheme so that the predicted cold pool and mesohigh agree best with the observations.

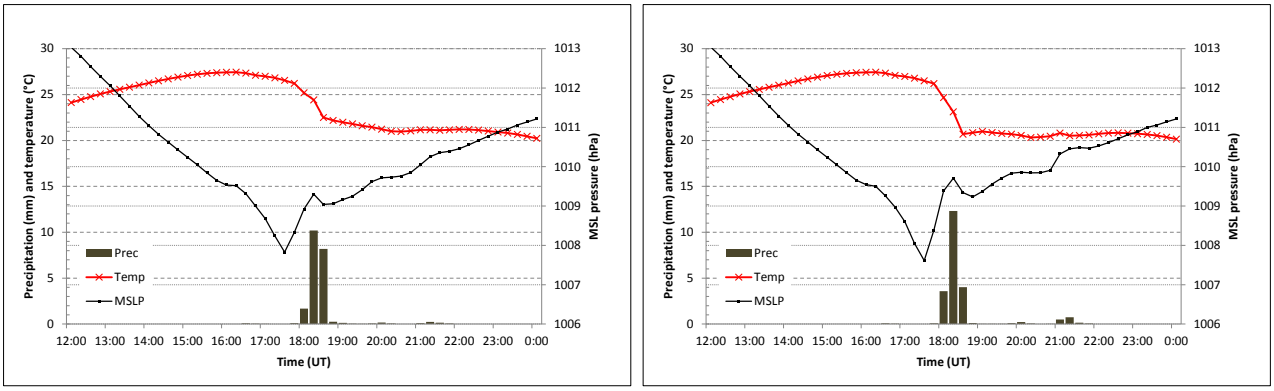

Figure 2: Simulated 2m temperature (°C, left vertical axis), MSL pressure (hPa, right vertical axis) and precipitation (mm, left vertical axis) in a single grid point in the modeled cold pool as predicted by BP40 (left) and BP40-tuned (right). The model run with reduced entrainment (BP40-tuned) shows a stronger cold pool and mesohigh.

A new simulation (BP40-tuned) has been run with reduced entrainment, in order to better predict the cold pool characteristics (figure 3). The cold pool and pressure perturbations have increased and show better agreement with observations. The peak temperature drop and pressure rise are now 7.4 K and 2.6 hPa. Moreover, the dewpoint in the cold pool has decreased and is more in agreement with observations. The mean wind speed and wind gusts have both increased at the edge of the cold pool; the peak wind gusts agree with those predicted by the reference run BP10 and are 20 m s^{-1}.

4.2 Downburst predictability

The downburst predictability has been assessed by selecting the highest mass flux at several times. The highest local mean downdraft mass fluxes predicted by BP40, BP40-tuned and BP10 are shown in Fig. 4. BP40 predicts a peak local mean downdraft mass flux of -1.1 kg $m^{-2}s^{-1}$, while BP40-tuned predicts a mass flux of -5.4 kg $m^{-2}s^{-1}$. The reference run predicts a peak mean downdraft mass flux of -4.7 kg $m^{-2}s^{-1}$.

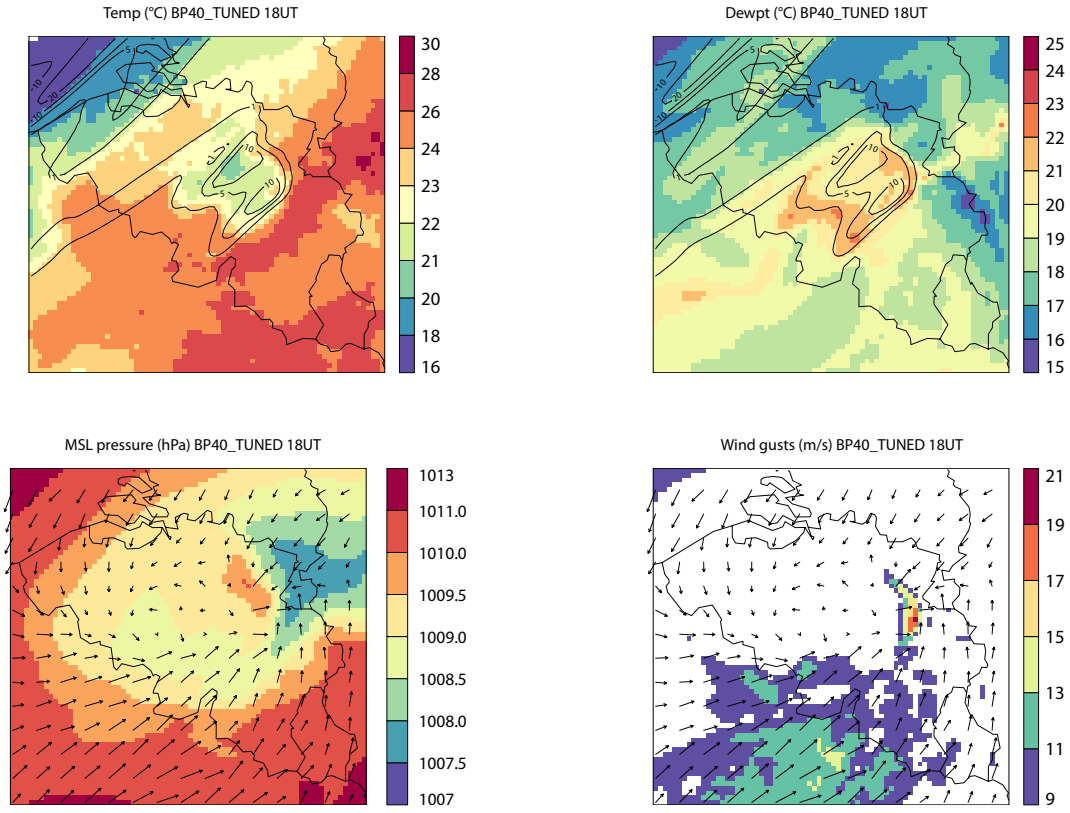

Figure 3: Forecast for 18 August 2011 1800 UTC by BP40-tuned, showing 2m temp. (°C) and 2m dewpoint (°C) with contours representing accum. prec. (lines for 1, 5, 10, 20, 50 and 100 mm), MSL pressure (hPa) with 10m wind arrows and wind gust speed (colors, in m s^{-1})

5 Final remarks

It has been found that a retuning based on the cold pool characteristics leads to (i) a downdraft more in agreement with the reference run, (ii) better storm outflow wind speeds, (iii) a more realistic representation of the dewpoints within the cold pools. We have done some additional tests where we compared the model skill of the new downdraft tunings with the original tunings over a test period of August 2011. From that, we conclude that the new tunings do not deteriorate the model skill.

References

Betts, A. K. and M. F. Silva Dias, 1979: Unsaturated downdraft thermodynamics in cumulonimbus. *J. Atmos. Sci.*, **36**, 1061-1071.

Bryan, G. H., J. C. Wyngaard, J. M. Fritsch, 2003: Resolution Requirements for the Simulation of Deep Moist Convection. *Mon. Wea. Rev.*, **131**, 2394-2416.

Carlson, T. N., E. H. Ludlam, 1968: Conditions for the occurrence of severe local storms. *Tellus*, **20**, 203-226.

De Troch, R., R. Hamdi, H. Van de Vyver, J.-F. Geleyn, and P. Termonia, 2013: Multi-scale performance of the ALARO-0 model for simulating extreme summer precipitation climatology in Belgium. *J. Climate*, **26**, 8895-8915, doi:10.1175/JCLI-D-12-00844.1.

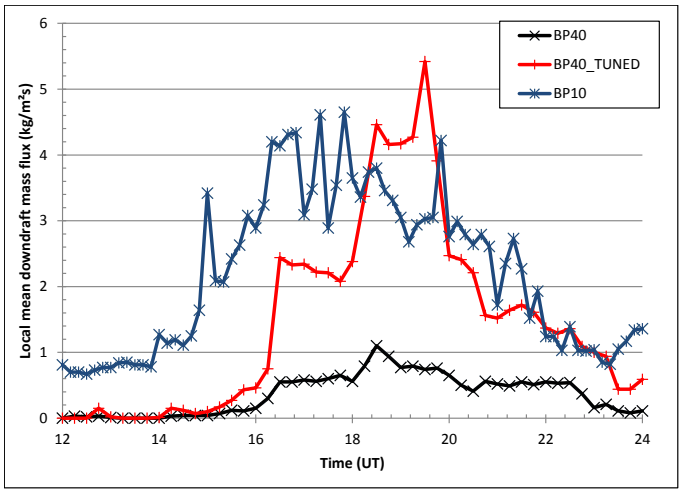

Figure 4: Peak local mean downdraft massflux (kg m − 2 s − 1) as predicted by BP40, BP40-tuned and BP10. Data every 15 min (for BP10: every 10 min) between 1200 UTC 18 August 2011 and 0000 UTC 19 August 2011.

Engerer, N. A., D. J. Stensrud, M. C. Coniglio, 2008: Surface characteristics of observed cold pools. *Mon. Wea. Rev.*, **136(12)**, 4839-4849.

Fujita, T. T., 1959: Precipitation and cold air production in mesoscale thunderstorm systems. *J. of Meteor.*, **16(4)**, 454-466.

Gerard, L., 2007: An integrated package for subgrid convection, clouds and precipitation compatible with the meso-gamma scales. *Quart. J. Roy. Meteor. Soc.*, **133**, 711-730.

Gerard, L., J.-M. Piriou, R. Brozkova, J.-F. Geleyn, D. Banciu, 2009: Cloud and precipitation parametrization in a meso-gamma-scale operational weather prediction model *Mon. Wea. Rev.*, **137**, 3960-3977.

Johnson, R. H. and P. J. Hamilton, 1988: The relationship of surface pressure features to the precipitation and airflow structure of an intense midlatitude squall line. *Mon. Wea. Rev.*, **116(7)**, 1444-1473.

Schmidt, J. M. and W. R. Cotton, 1989: A high plains squall line associated with severe surface winds. *J. Atm. Sci.*, **46(3)**, 281-302.

Sud, Y. C. and G. K. Walker, 1993: A rain evaporation and downdraft parameterization to complement a cumulus updraft scheme and its evaluation using GATE data. *Mon. Wea. Rev.*, **121(11)**, 3019-3039.

van Delden, A. , 1998: The synoptic setting of a thundery low and associated prefrontal squall line in western Europe. *Meteorol. Atmos. Phys*, **65**, 113-131.

Vescio, M. and R. Johnson, 1992: The surface-wind response to transient mesoscale pressure fields associated with squall lines. *Mon. Wea. Rev.*, **120(9)**, 1837-1850.

Wakimoto, R. M., 1982: The life cycle of thunderstorm gust fronts as viewed with Doppler radar and rawinsonde data. *Mon. Wea. Rev.*, **110**, 1060-1082.

Weisman, M. L., W. C. Skamarock and J. B. Klemp, 1997: The resolution dependence of explicitly modeled convective systems. *Mon. Wea. Rev.*, **125**, 527-548.

The fog above sea problem in Harmonie: Part 1 Analysis

Wim de Rooy
Acknowledgements: Emiel van der Plas, Geert Lenderink, Jan Barkmeijer

Introduction

A few years ago the Harmonie model was gradually introduced in our operational practice at KNMI. Since the start it has proven its value, especially in cases of extreme weather. There are however still important deficiencies. During the cloud and convection workshop in Norrköping October 2012, high priority was given to the fog above sea problem. Several times and at different institutes, Harmonie produced large and persistent fog fields above sea, which were not observed. Especially in The Netherlands these unrealistic fog fields are problematic as our main airport is located close to the coast. Besides, these erroneous fog fields decrease the credibility of the model to customers and forecasters. Several physical processes and parameterizations can contribute to the formation of fog. Here we present an analysis of some of the most plausible processes related to the production of excessive fog.

Analysis of the problem

Many of the sensitivity tests in this paper are based on a test case starting at 22 March 2012 at 12 UTC. In observations almost no fog was present (see Fig. 1 for the next day at 11:14 UTC). However, the model run shows two interesting fog fields above the North Sea; one large fog field already present in the beginning of the run and subsequently advected towards the south west, and a fog field that is developed during the 24h run in the southern part of the North Sea (see Fig. 2). Tests are done with a cold and warm start (assimilation run started at 15 March 2012).

Movies of the complete 24h run (and results of many other experiments) can be downloaded from:
https://hirlam.org/trac/wiki/HarmonieWorkingWeek/Clouds201210
under section “Preliminary results North Sea fog case”.

Figure 1: Modis vis satellite image valid for 23 March 2012 at 11:14UTC, showing almost no fog above the North Sea. Fog is also absent in the previous 24 hours whereas in the next 24 hours the fog field near the coast of Denmark is expanding towards the North Sea.

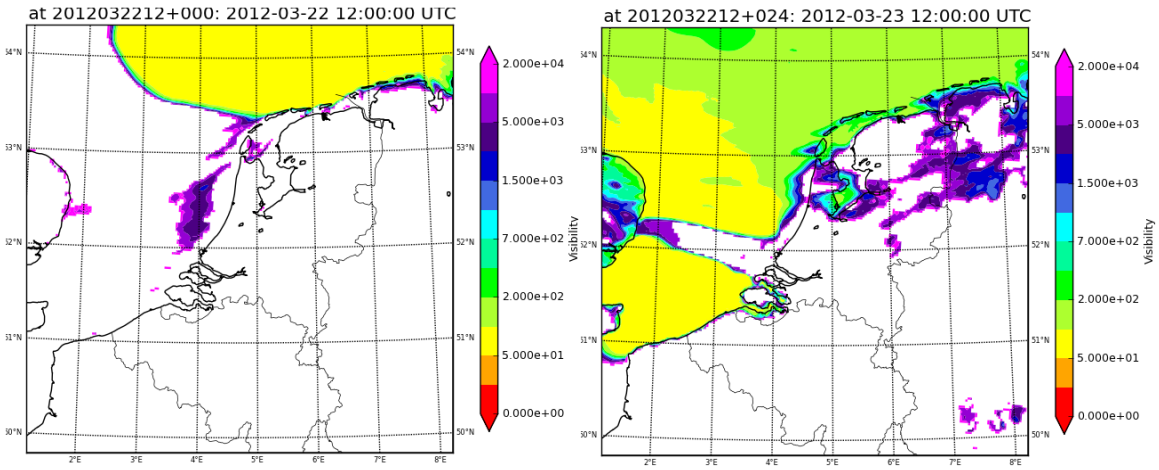

Figure 2: Showing the +0 (left panel) and +24h (right panel) visibility [m] forecast of Harmonie started at 22 March 2012 12 UTC in the default setting and using a warm start.

Sensitivity tests for the following model components, potentially related to fog above sea, are performed:

1. Sea surface
2. Convection scheme
3. Cloud scheme
4. Turbulence scheme

Ad 1)
First of all, the Harmonie SST is checked against satellite observations. Conclusion is that the SST might be slightly too high. Because a higher SST would lead to less fog (this is verified), errors in the SST can be excluded as cause of the fog problem.

Hereafter, we investigated the quality of the surface fluxes. Deficiencies in the surface fluxes could arise from an inadequate parameterization or incorrect surface and/or lowest model level meteorological parameters. Unfortunately, no direct observations of the surface fluxes were available. Nevertheless, the parameterization could be validated by using the surface and lowest model level as input for the so-called fluxroutines [1)]. Especially above sea these fluxroutines provide accurate estimates of the surface fluxes provided the input is accurate. For a location in the southern part of the North Sea where fog develops, we see moistening occurs during the night until the atmosphere becomes fully saturated and subsequently the conditions become unstable (see Fig. 3a). From this moment the convection scheme will be active. As shown in Fig. 3b the modeled surface fluxes are in reasonable agreement with the fluxroutine output. Moreover, the observed differences would result in less fog and can therefore not explain the erroneous fog fields.

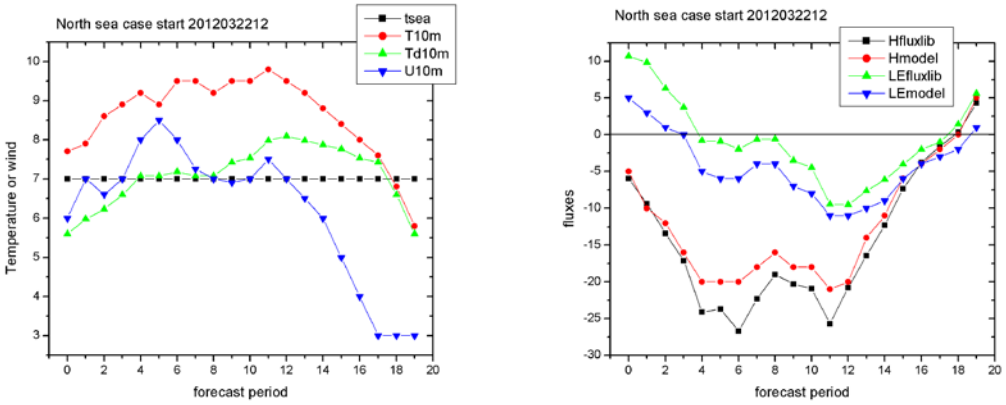

Figure 3: Temperature, dewpoint temperature and wind speed (left panel) and surface fluxes (right panel) as a function of the forecast period for a location in the southern part of the North Sea in the middle of the developing fog field. Hfluxlib and LEfluxlib are estimates of respectively the sensible and latent heat flux using the fluxroutines. Upward fluxes have positive values.

Finally, tests with different surface scheme options (ECUME, DIRECT, canopy scheme on/off) revealed no substantial impact on the formation of fog above sea.

Ad 2)
Runs with additional output showed (as expected) that the edmfm convection scheme is not active before and during the development of fog. Only when the fog is well developed and becomes dense, the convection scheme becomes active. From then on the conditions are diagnosed as stratocumulus by the convection scheme, resulting in the use of moist updrafts only (no dry updraft). Increasing the convection for this stratocumulus regime has no substantial effect.

Tests with the edkf convection scheme in combination with no extra variance term (the default) showed that the development of fog starts somewhat earlier and the positive feedback loop to more dense fog is somewhat stronger. Overall, it seems highly unlikely that the solution of the fog problem can be found in the convection scheme.

Ad 3)
The cloud scheme determines the cloud fraction and the liquid/ice water content. Key parameter is the variance of the distance to the saturation curve. When using the full statistical cloud scheme, there are contributions to the variance from the turbulence and the convection as well as an additional variance term as described in [2)]. Runs have been performed with all these contributions to the variance as separate output. Striking is the correlation between the contribution due to turbulence and reduced visibility during the first half of the 24h simulation (see Fig. 4). Note the following positive feedback loop: the production of TKE increases the variance, which in turn increases the liquid water content, which increases the radiative cooling and consequently TKE increases.

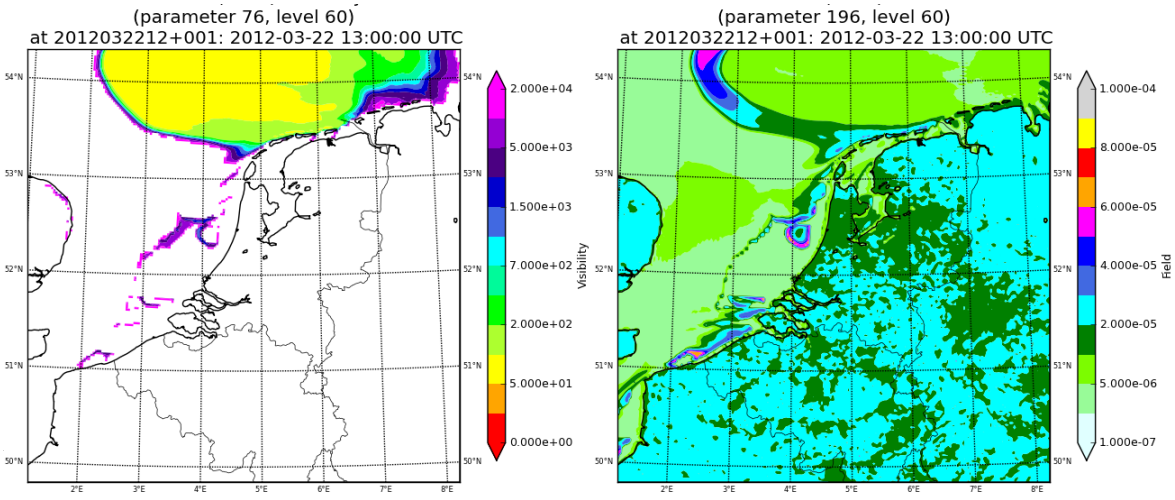

Figure 4: Showing the +1h Harmonie forecast of visibility [m] (left panel) and variance contribution from the turbulence only (right panel) started at 22 March 2012 12 UTC.

If we remove the contribution of the turbulence to the variance and reduce the extra variance term (proportional to 0.005 q_{sat} i.o. 0.02 q_{sat}) the fog field in the north remains the same but in the south no fog or reduced visibility is formed until fog above land is advected with the easterly winds to sea. Subsequently this fog “explodes” above sea (as observed before in harmonie forecasts by Sander Tijm). In Fig. 5 the start of this process is shown. We will return to this phenomenon in part II of this paper as it nicely illustrates the likely cause of this fog problem.

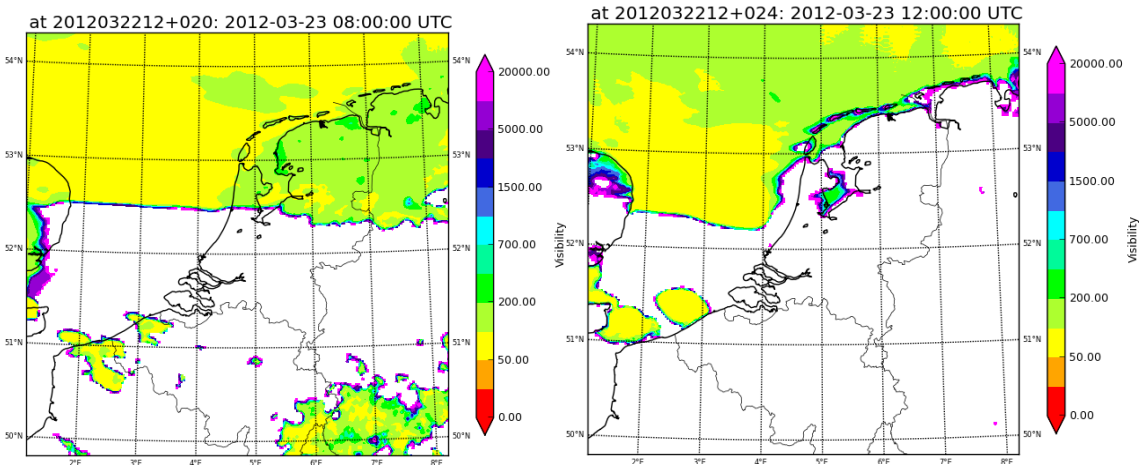

Figure 5: Cold run 2012032212 +20h (left) and +24 (right) without the contribution to the variance of the turbulence scheme and a reduced extra variance term. Near the coast of Belgium fog develops above land and is subsequently advected above sea where it spreads out rapidly whereas the corresponding fog fields above land are dissolved

Ad 4)
The turbulence scheme potentially plays an important role in the forming and dissolving of fog as it determines the vertical mixing due to isotropic turbulence. The turbulence scheme should provide the primary mechanism, namely top entrainment, to dissolve the fog field by entraining relatively warm and dry air. Looking at a vertical slice through the fog field above sea (see Fig. 6), the turbulent activity (indicated by the TKE) is very small (or virtually non existent) in the upper part of the fog layer. This is an indication that the turbulence scheme is not capable of dissolving the fog.

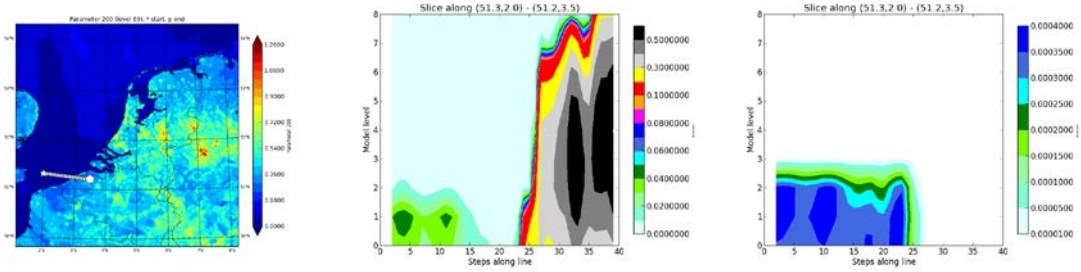

Figure 6: Vertical slices of TKE (middle panel, in m^2/s^2) and cloud water (right panel, in kg/kg) along the line as indicated in the left panel starting at the star (above sea) and ending at the pentagon (above land). The +24h forecast of a cold start at 2012032212 is shown. In the left panel the TKE at the lowest model level is plotted.

To investigate the sensitivity of the model to the turbulence scheme several experiments are done. Changes in the constants of the stability functions (to Schmidt & Schumann settings) did not result in significant impact. On the other hand, multiplying the turbulent length scale with 2 resulted in a large impact (although length scales are pretty small in the developing stage of the fog). The existing fog field in the north becomes less dense and the developing fog field in the southern part is substantially reduced (not shown).

Apparently, the development of fog can be very sensitive to the settings in the turbulence scheme. However, simply tuning the turbulence scheme to this fog case would undoubtedly lead to

problems with other parameters or other conditions. Moreover, how can we know the turbulence scheme is really the cause of the problem? We might simply compensate for the real cause by retuning the turbulence scheme. Fortunately (thanks to Eric Bazile), Arome and Harmonie participated in the ASTEX intercomparison case. In this lagrangian case describing a rising stratocumulus which finally breaks up, several processes are prescribed (according to observations) and detailed observations as well as LES output is available. Consequently, this case can show us some real deficiencies of parameterizations.

Fig. 7 reveals that apart from not breaking up, the stratocumulus layer stays too low. In the version with EDKF convection (not shown) the stratocumulus layer reaches higher altitudes because the excessive mixing convection scheme results in strong top entrainment (Harmonie runs without convection show almost no top entrainment). However, for the majority of the simulation the top entrainment is induced by the cloud radiative cooling at the top of the cloud layer and it is the turbulence scheme that should represent this. Later on in the simulation shallow convection enters the cloud layer and starts to contribute to the top entrainment and breaking up.

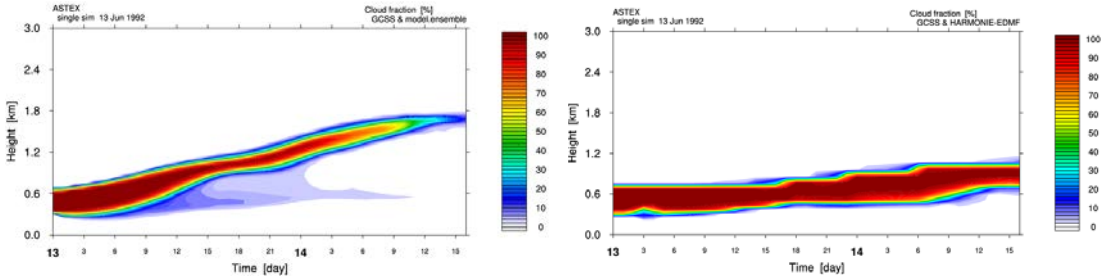

Figure 7: Contourplots of cloud fraction as a function of the simulation hour during the ASTEX case (see text) from LES runs (left panel) which can be considered as observation, and with Harmonie using edmfm.

Based on ASTEX we can conclude that the turbulence scheme of Harmonie underestimates the top entrainment in this situation. This underestimation can have a relation with our fog problem. Moreover, too little top entrainment can also explain the underestimation of cloud base and boundary layer height as often observed in Harmonie. Finally, more top entrainment will generally lead to less stratus and our operational experience is that Harmonie often overestimates stratus. These links between known deficiencies of the operational model and results in well-controlled intercomparison (1D) cases are extremely valuable for practical and scientifically sound model improvement.

Instead of tuning the current scheme we might incorporate a new scheme which is used successfully for many years in the KNMI RACMO (Regional Climate MOdel). This climate model, which uses the same (edmfm) convection scheme as Harmonie but a different turbulence scheme, clearly performs better for ASTEX, showing more top entrainment. Like the current scheme, this TKE scheme uses a 1½ order closure, but a different length scale formulation of Lenderink & Holtslag [3] as well as different details in the TKE prognostic budget equation and the eddy diffusivity formulation. Note that in Hirlam we followed a similar road going from a Bougeault & Lacarerre [4] to a Lenderink Holtslag [3] length scale formulation.

In the next newsletter we will describe the implementation of and the experiences with the RACMO turbulence scheme in Harmonie. Besides, more insight of the processes leading to the erroneously developing fog field will be given.

Conclusions and outlook

Several processes potentially related to the fog above sea problem are investigated. Many of these processes can be excluded, or are at least unlikely to be the cause of the overestimation of fog. However, ASTEX clearly reveals that the Harmonie turbulence scheme has too little top entrainment. Too little top entrainment can explain several deficiencies of Harmonie, such as the fog problem. At the same time results of Harmonie for the North Sea fog case turned out to be quite sensitive to the settings in the turbulence scheme. Based on these arguments we continue our investigation focusing on the turbulence scheme, as described in part II of this paper published in the next newsletter.

References

[1)] van Ulden, A.P., and A.A.M. Holtslag, 1985: Estimation of atmospheric boundary layer parameters for diffusion applications. *J. Climate Appl. Meteor.*, **24**, 1196-1207

[2)] de Rooy, Wim, Cisco de Bruijn, Sander Tijm, Roel Neggers, Pier Siebesma, Jan Barkmeijer, 2010: Experiences with Harmonie at KNMI. Hirlam Newsletter no. 56, November 2010

[3)] Lenderink, G. and A.A.M. Holtslag, 2004: An updated length scale formulation for turbulent mixing in clear and cloudy boundary layers. *Q. J. R. Meteor. Soc.*, **130**, 3405-3427

[4)] Bougeault P., Lacarrere P., 1989: Parametrization of orography-induced turbulence in a mesobetascale model. *MWR*, **117**, 1872-1890.

Evaluation of increased horizontal and vertical resolutions in AROME-France deterministic forecasts for convective events

Yann Seity, Didier Ricard, Julien Léger, Mirela Pietrisi

Introduction

For several decades, the increase of numerical weather prediction systems resolution has followed the increase of computing power. A major jump was achieved a few years ago for operational models, switching from parameterized to explicitly resolved deep convection with horizontal resolution below 4 km. In Météo-France, the next resolution increase is expected soon: by the beginning of 2015, our operational deterministic 2.5 km 60 levels (L60) AROME forecasts (Seity et al., 2011) will be replaced on a new supercomputer, by 1.3 km 90 levels (L90) ones. Preparatory work started in 2012 by the choice of the lowest model level altitude (5m versus 10m as currently) with the best compromise between a reduced time step and the quality of model forecasts, particularly on fog events. In this configuration, model time step has been reduced from 60 to 45s, with the use of an iterative centred implicit (ICI) time-scheme with one iteration (Bénard, 2013). After some tests, we chose a regular vertical resolution increase between L60 and L90 AROME. Daily experimental AROME runs at 1.3 km have been setup on a reduced domain (Figure 1) and have operated since 1st June 2012. AROME-1.3km L90 is setup and hourly boundary coupled by operational AROME-France-2.5km. It performs 30-h forecasts starting at 00 UTC. A reference version of AROME-2.5km L60 runs under the same conditions, over the same geographic domain.
In 2013, meteorological evaluation started. This paper gives some highlights on the impact of the increased resolution in AROME for convective events.

Evaluation of rainfall patterns

At 1.3km resolution, convective cells seem to be globally less active but more numerous than at 2.5 km (Figure 1). We will now try to quantify objectively this observation, by using a cell tracking algorithm based on the RDT (Rapid Thunderstorm Detection) system (Morel et al., 2002).

48 days were selected between June and November 2012, based on their high lightning activity over France. We hourly applied the cell tracking algorithm on observed radar reflectivities and simulated ones for AROME-2.5km L60 and AROME-1.3km L90. We then derived some statistics on convective cells (Figure 2). AROME simulated radar reflectivities are defined as the maximal value between 1500, 2000 and 2500m heights.

AROME-2.5km L60 clearly underestimates the number of convective cells during all the diurnal cycle (Figure 2a). It particularly underestimates the number of small cells, overestimates the number of large ones (Figure 2b) and underestimates the cells maximal intensity (Figure 2c).

AROME-1.3km L90 is closer to radar observations (for the timing, intensity and size). The diurnal peak in terms of number of cells is observed 2 hours after the one simulated by AROME runs, but the number of cells is remarkably similar between RADAR and AROME-1.3km L90 (Figure 2a). AROME is not able to simulate the highest values of radar reflectivities (Figure 2c). This could be explained by the radar simulator applied on model fields (hypothesis on particule size distribution for instance), and also by the fact that hail is not explicitly represented in the model. The secondary peak

at 04 UTC is not captured by AROME. Compared to the main peak in the afternoon, it contains a much larger proportion of very small cells, which are not well simulated by the model.

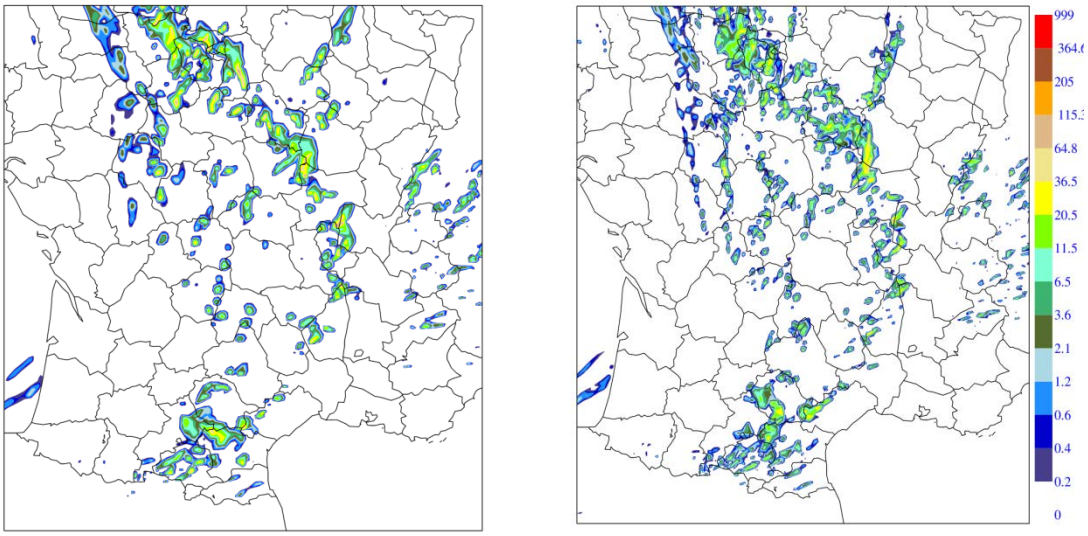

Figure 1: 1500m precipitation rate (mm/h) at 1330 UTC 21 June 2012: AROME-1.3km L90 (right) and AROME-2.5km L60 (left).

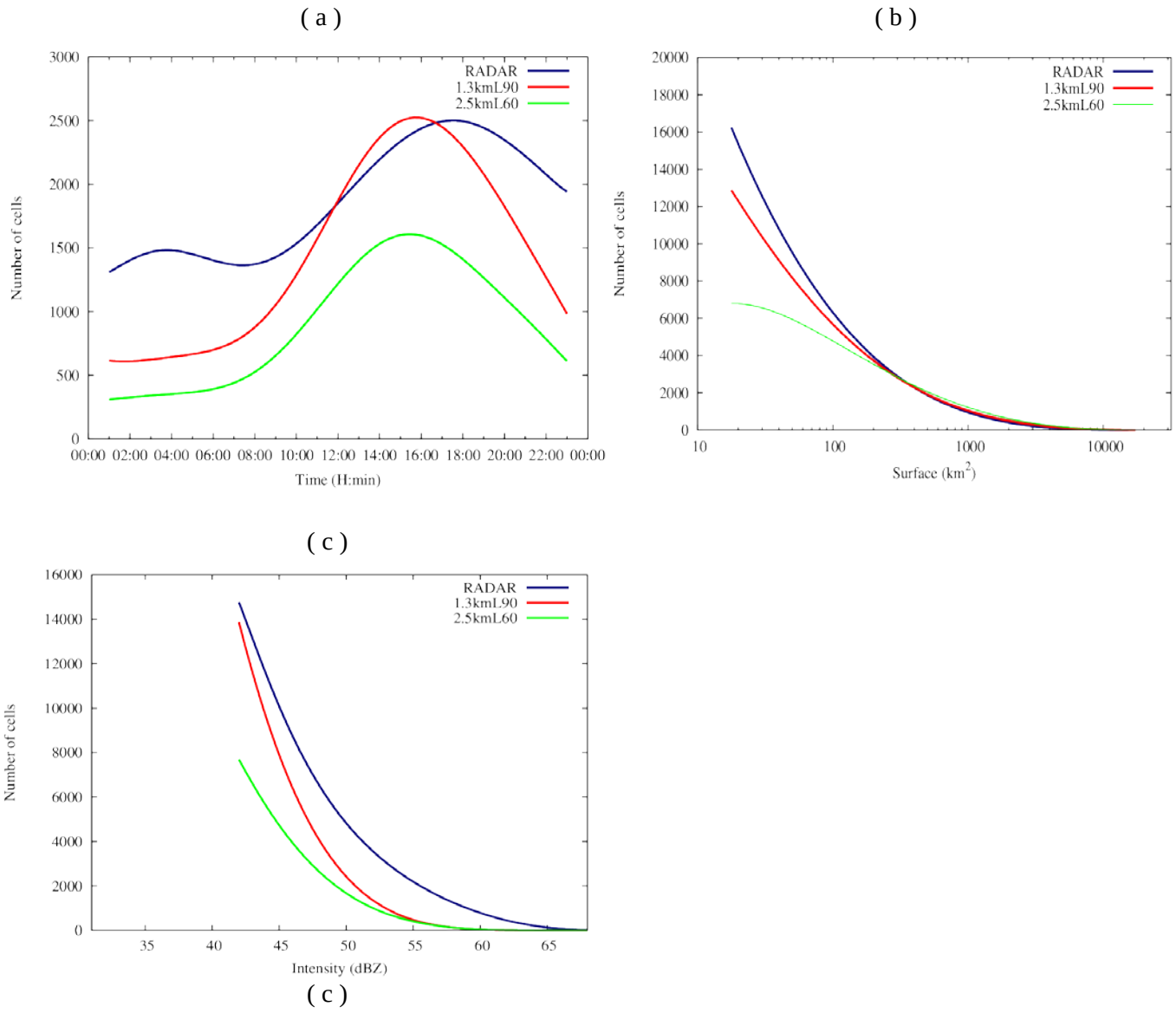

Figure 2 : Cell statistics over the 48 convective days using a detection threshold of 41 dBZ: (a) diurnal cycle, (b) cell size (km²) and (c) maximal intensity (dBZ).

Conclusions

By the statistical study of 48 convective days, we have shown that AROME-1.3km L90 provides more realistic convective cells than AROME-2.5km L60. They are more numerous and more intense at 1.3km. At 2.5km, the AROME model produces too large cells.

Consequences on rainfall scores have to be studied in details, for different seasons, but a significant improvement is expected, at least in summer, due to more realistic cell statistics. Some interesting statistics could also been computed on cell lifetime, by using 15 minutes data instead of hourly ones. In 2014, evaluation and tunings of the model will continue, in parallel with the development of the 1.3km assimilation part, in order to be able to launch an E-suite in summer which will also contain a resolution increase in AROME's coupling model: ARPEGE.

Acknowledgments : *We particularly thank Thibaut Montmerle for his technical help on the RDT software.*

References :

Bénard, P., 2003 : Stability of semi-implicit and iterative Centred-implicit time discretizations for various equations systems used in NWP, Monthly Weather Review, 131, 2479-2491.

Morel, C., S. Sénési, and F. Autones, 2002: Building upon SAF-NWC products: Use of the Rapid Developing Thunderstorms (RDT) product in Météo-France nowcasting tools. Proceedings, The 2002 Meteorological Satellite Data Users' Conference,Eumetsat and Met Eirean, Dublin, Ireland, 248-255.

Seity, Y., P. Brousseau, S. Malardel, G. Hello, P. Bénard, F. Bouttier, C. Lac, and V. Masson, 2011 : The AROME-France convective-scale operational model. Monthly Weather Review,139 (3), 976–991.

Divergence in limited-area models for numerical weather prediction

Extended abstract of the doctoral thesis, September 2013

Author: Vanja Blažica, University of Ljubljana, Faculty of Mathematics and Physics

Supervisor: prof. Nedjeljka Žagar

Introduction

Our fundamental understanding of atmospheric dynamics, based on the quasi-geostrophic theory, although applicable for the synoptic scales, does not work well for the mesoscale. Here, numerous ageostrophic and non-hydrostatic processes (e.g. convection) take place. Understanding their dynamics requires taking equally into account both vorticity and divergence, i.e. both quasi-geostrophic and inertio-gravity motions. Although it is well understood that importance of divergence increases as we move to shorter scales, little is known about the distribution of divergent energy at scales around 100 km and smaller and about its distribution in the middle and the lower troposphere. The topic of this research is therefore the distribution of atmospheric energy between the divergent and rotational motions on the mesoscale through use of kinetic energy spectra. Performing this research in the operational limited-area model ALADIN has posed several challenges and these are explored in depth. In particular, the thesis addresses one of major issues in the formulation of the spectral LAMs: the problem of periodization of the generally non-periodic limited-area fields.

The following more specific questions are addressed:

- In view of the non-trivial preparation of the limited-area model spectra, how do different methods for periodization influence the properties of the spectra?
- What is the average contribution of divergent kinetic energy with respect to rotational energy in the ALADIN/SI model?
- How does the energy partitioning between divergent and rotational energy change at different altitudes as the horizontal scale becomes smaller?
- What are the properties of the rotational and divergent kinetic energy spectra in relation to the model initialization and the spin-up process?

The impact of methods for periodization on the spectra

The impact is estimated by performing a simplified experiment, in which the simulated fields to be periodized have a known spectrum. The fields are constructed in spectral space, including random perturbations, and transformed to grid-point space, where the periodization is performed. The fields are then transformed back to spectral space and their new spectrum is compared to the original one.

The impact of the periodization method can therefore be seen as a departure from the prescribed spectrum.

The methods under consideration are the extension zone with trigonometric functions (as used in HIRLAM), the extension zone with spline functions (as used in ALADIN), the extension zone using the Boyd method (also adopted in ALADIN), the detrending and the discrete cosine transform.

The kinetic energy spectra of the treated fields (Fig. 2) show that the detrending, the discrete cosine transform and the Boyd method produce the spectra similar to the original one. For the periodization with trigonometric functions and spline functions the departure from the original spectrum depends on the width of the extension zone. This research suggests that when studying the spectra of a limited-area model, a narrower extension zone is preferred, if not at all avoided. The original HIRLAM and ALADIN algorithms should not be applied over wide extension zones since the constraint on preservation of normal gradients together with the selected extrapolation functions leads to strong amplification of variations inside the extension zone.

The excess energy deforms the shape of the spectra at all scales. The position of the bump in the large-scale part of spectrum is related to the width of the extension zone; its source is the large values in the top right corner of the periodized grid-point field (Fig. 1). The shorter scale noise is a consequence of treating the matrix line-by-line, column-by-column. This excess energy is efficiently removed by the smoothing filter, applied in ALADIN, but even after this correction the spectrum does not match the original – it remains too steep.

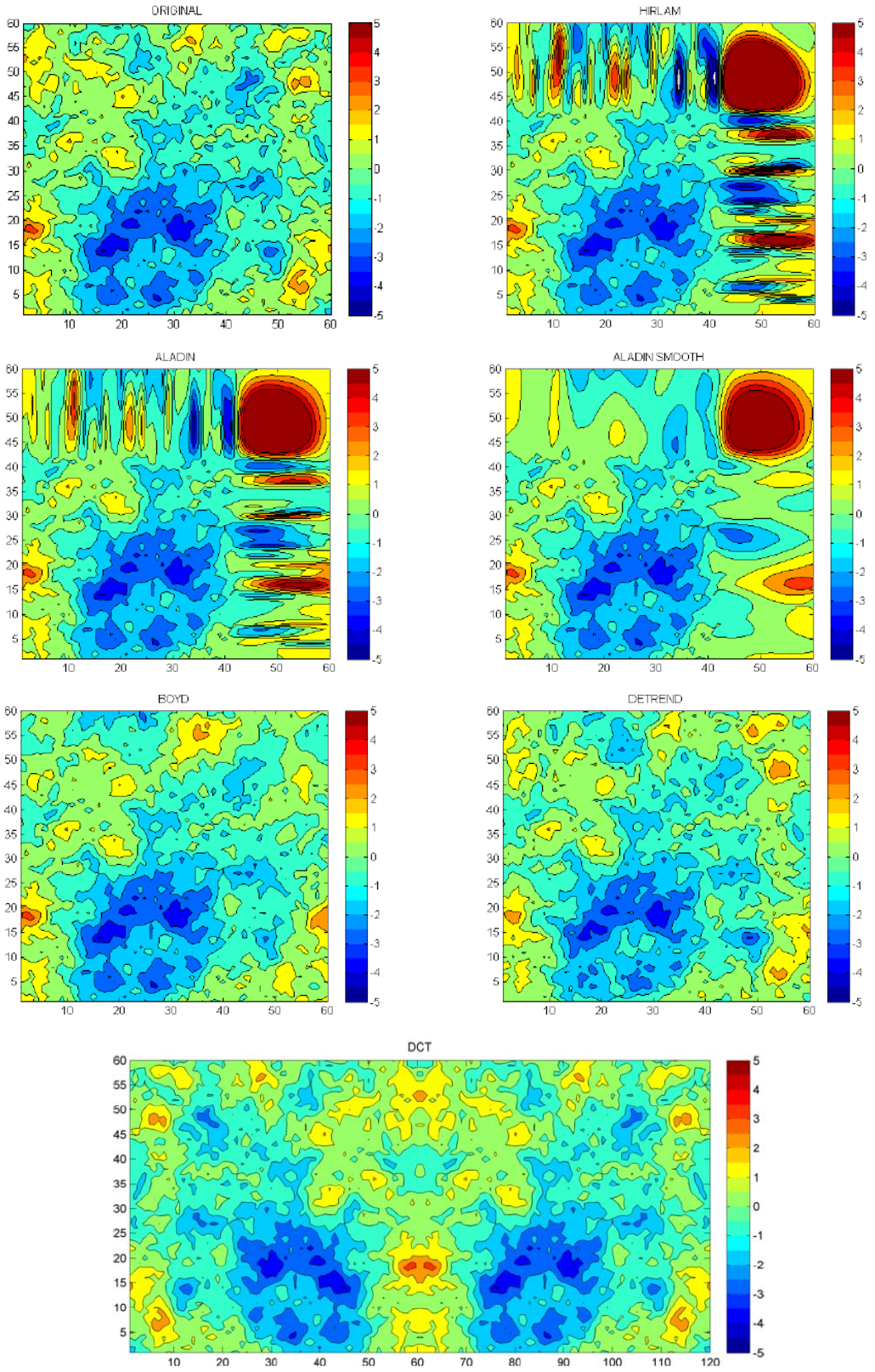

Figure 1: The arbitrary 2D wind fields (with $K^{-5/3}$ spectrum) in grid-point space before (top left) and after the periodization for the discussed methods. For ALADIN, the fields are shown before and after the application of the 2D smoothing operator. For the discrete cosine transform (DCT), only the periodization in x-direction is shown.

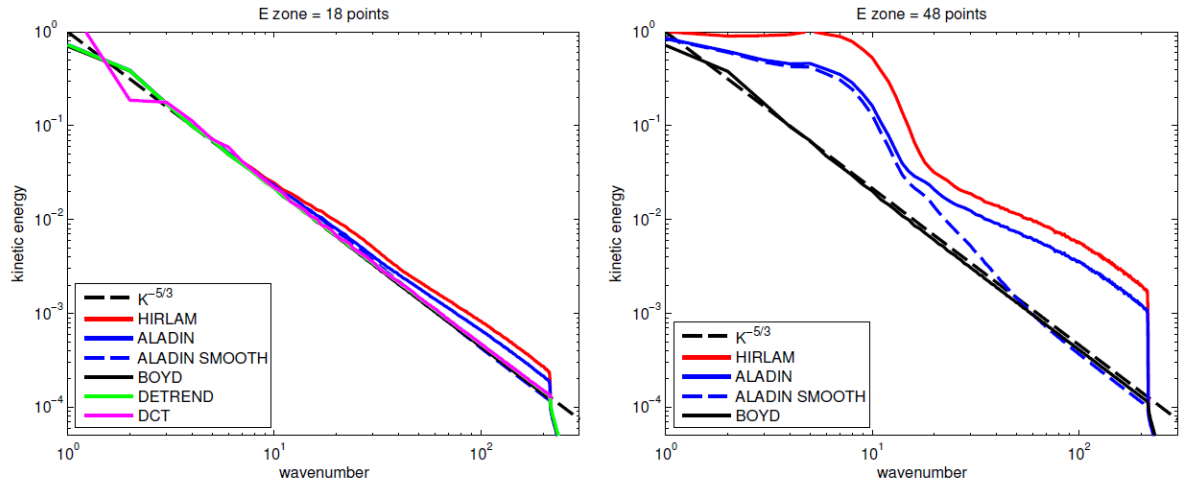

Figure 2: Kinetic energy spectra for all the discussed methods. For methods that make use of the extension zone, the results are presented for a narrower zone with 18 points (left) and for a wider zone with 48 points in the extension zone (right). The domain size is 432 x 432 points.

Kinetic energy spectra in the ALADIN model

The central research for this thesis makes use of the ALADIN/SI forecasts of vorticity and divergence fields. The results have been published in Blažica et al. (2013). The investigation period is July 2007; forecasts are generated twice a day starting at 6 and 18 UTC. The model domain is centred over Slovenia and covers most of the continental Europe and the central part of the Mediterranean. The domain dimensions are L_x=1930 km and L_y=1850 km. The horizontal grid spacing is $\Delta x=\Delta y$=4.4 km. In the vertical, there are 43 model levels up to 5 hPa. The width of the extension zone is 11 points. The time step for the semi-Lagrangian integration is 180 s. The model version is CY35T1 with 3MT physics package. The initial conditions are obtained by downscaling the ECMWF analyses, which are results of a 12-hour 4D-Var that applies a T95 inner loop minimization and a T255 outer loop, and the digital filter is applied. The spectra are computed using the detrending method, in accordance with the findings of the simplified experiment.

The results show that through most of the troposphere, the kinetic energy spectrum at scales around 100 km and smaller is reasonably well characterized by the $K^{-5/3}$ power-law, matching the spectra from high-altitude observations by aircrafts (Fig. 3). In the boundary layer, the spectrum becomes shallower, indicating the importance of the orography forcings.

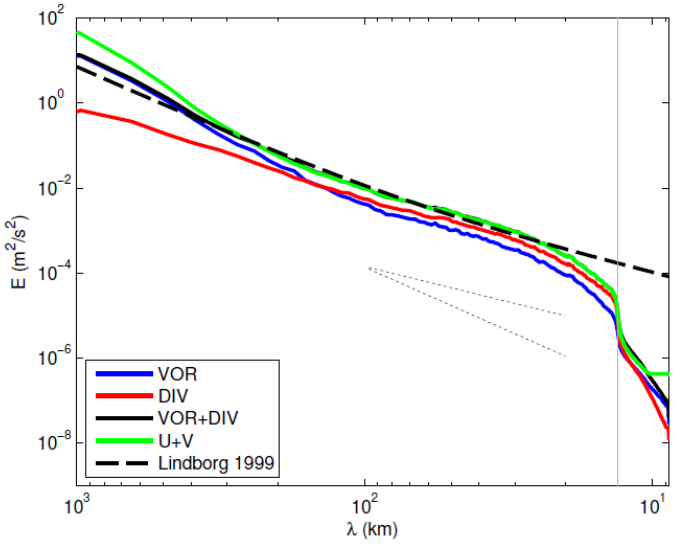

Figure 3: ALADIN energy spectra, averaged over model levels between 9 and 11 km. VOR denotes rotational kinetic energy, DIV divergent kinetic energy, VOR+DIV denotes total kinetic energy as a sum of rotational and divergent components while U+V denotes stands for total kinetic energy computed from the velocity components. The black dashed line is the Lindborg (1999) functional fit to the aircraft data. The vertical grey line denotes 3Δx. Short dotted lines have slopes of K^{-3} and $K^{-5/3}$.

At scales below 300 km, about 50% of kinetic energy in the free troposphere is divergent energy. The percentage increases towards 70% at the surface and in the upper troposphere towards 100 hPa. In two layers, at approximately 900 hPa and between 500 hPa and 400 hPa, rotational energy dominates on all scales larger than the model effective resolution found to be at about 6Δx. At all levels, the divergent energy spectra are characterized by shallower slopes than the rotational energy spectra.

The maximal percentage of divergent energy in the total kinetic energy at the same level is found at stratospheric levels around 100 hPa and at scales below 100 km, which are not represented by the global models analysed so far (Fig. 4). This result calls for further studies with high-resolution models and comparisons with observations. A similar divergent energy distribution is found also for several other versions of ALADIN and also for the HARMONIE model and a grid-point version of the HIRLAM model.

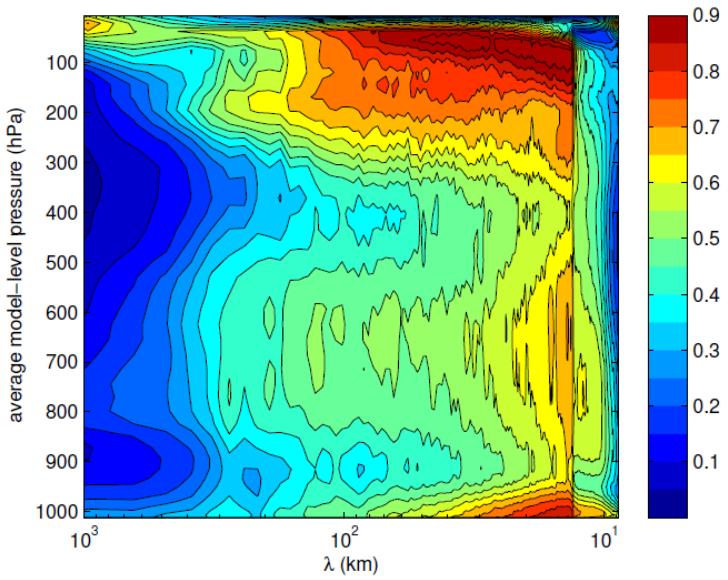

Figure 4: Distribution of divergent energy contribution with respect to altitude and horizontal scale. Divergent energy is expressed as the fraction of the total kinetic energy at each model level. Contour interval is 0.05 (5%).

Spectra during the spin-up process

Finally, this research investigates the spin-up process in the ALADIN model by presenting the rotational and divergent energy spectra during the first hours of forecast. It is shown that the spin-up process is faster for the divergent component of the model circulation, most likely due to faster propagation of inertia-gravity waves generated either by the downscaling process or an imperfect initialization procedure. The amount of the kinetic energy added during the early stage of the forecast is larger for divergent energy than for rotational energy and closer to the ground, due to orographic forcing and possibly also due to applied numerical diffusion.

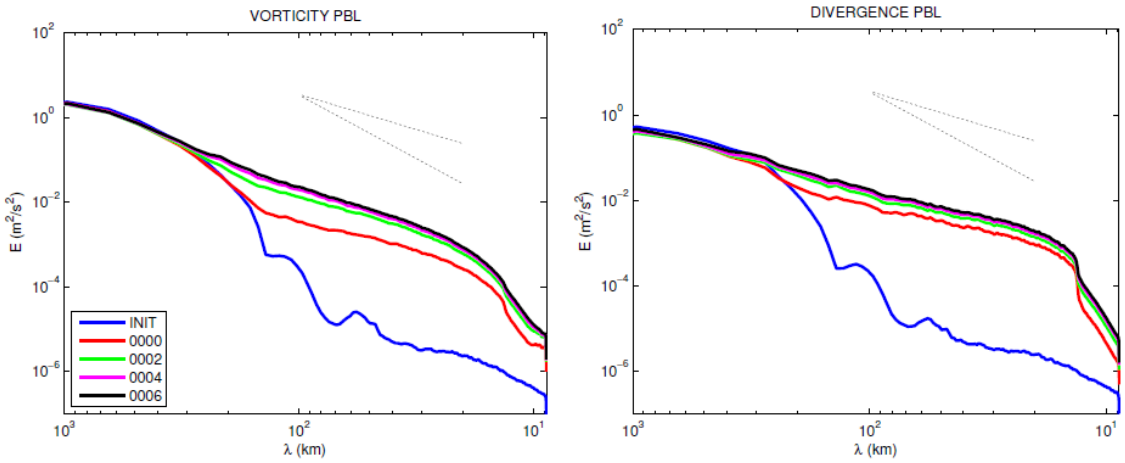

Figure 5: ALADIN spectra of rotational and divergent kinetic energy for the first six hours of forecast, vertically averaged over model levels in the PBL. INIT denotes the spectra of the downscaled fields while 0000 denotes the spectra after the DFI.

Outlook

Divergence is a control variable in data assimilation in mesoscale NWP models meaning that the energy spectra of analysis increments are greatly influenced by the imposed balance constraint in the background-error term for data assimilation. The question arising from our study is therefore whether similar results regarding the distribution of rotational and divergent energy in the analysis and forecast fields would also be obtained for the forecast-error fields. For now, the error growth is assumed to be linear (Berre, 2000), which is in principle a good approximation for the synoptic scales, yet this is not necessarily true for the mesoscale (Tribbia and Baumhefner, 2004). Therefore our ongoing research studies possible differences in error growth between vorticity and divergence fields and possible relation of error spectra with the spectra of the basic fields.

Bibliography:

Berre, L. Estimation of synoptic and mesoscale forecast error covariances in a limited-area model. Mon. Wea. Rev. 128, 644–667 (2000).

Blažica, V., Žagar, N., Strajnar, B., Cedilnik, J. Rotational and divergent kinetic energy in the mesoscale model ALADIN. Tellus A 65, 18918 (2013).

Lindborg, E. Can the atmospheric kinetic energy spectrum be explained by two-dimensional turbulence? J. Fluid Mech. 388, 259–288 (1999).

Tribbia, J., Baumhefner, D. P. Scale interactions and atmospheric predictability: An updated perspective. Mon. Wea. Rev. 132, 703–713 (2004).

AROME in AUSTRIA

Xin Yan, Christoph Wittmann and Florian Meier

1 Introduction

AROME 2.5km forecast system including 3DVAR assimilation was set up at ZAMG in addition to the operational ALARO 5km model and is now reaching an operational status. In this article, the basic configuration of AROME/3DVAR will be first introduced (section 2). Then an example of this year's flash floods case study will be showed (section 3) to demonstrate the ability of AROME in fine scale precipitation forecast. After that the impacts of additional test experiment of GPS assimilation are shown as well (section 4).

2 The AROME/3DVAR system in Austria

2.1 **Basic model configurations**

The main characteristics of the current AROME system at ZAMG can be summarized in the following table.

Table 1: Model setup

Model version	CY36T1 (3DVAR) /CY37T1op1 (production)
Resolution	2.5km
Levels	60/90 (Fig. 2)
Area	operational: 432 x 320 (small domain) experimental: 600 x 432 (big domain) Fig. 1
Coupling model	IFS
Initial conditions	3DVAR + OI (soil)
Surface scheme	Reference 7.1
Starting times	00/03/06/09/12/15/18/21 UTC
Cycle interval	3 hours
Forecast range	30 hours

In addition to the operational system, a parallel AROME suite is maintained and run on an extended domain (see Figure 1) in a test mode. Beside the domain size, the number of vertical levels has been increased from 60 to 90 for this parallel version. It is planned to switch to this version in 2014.

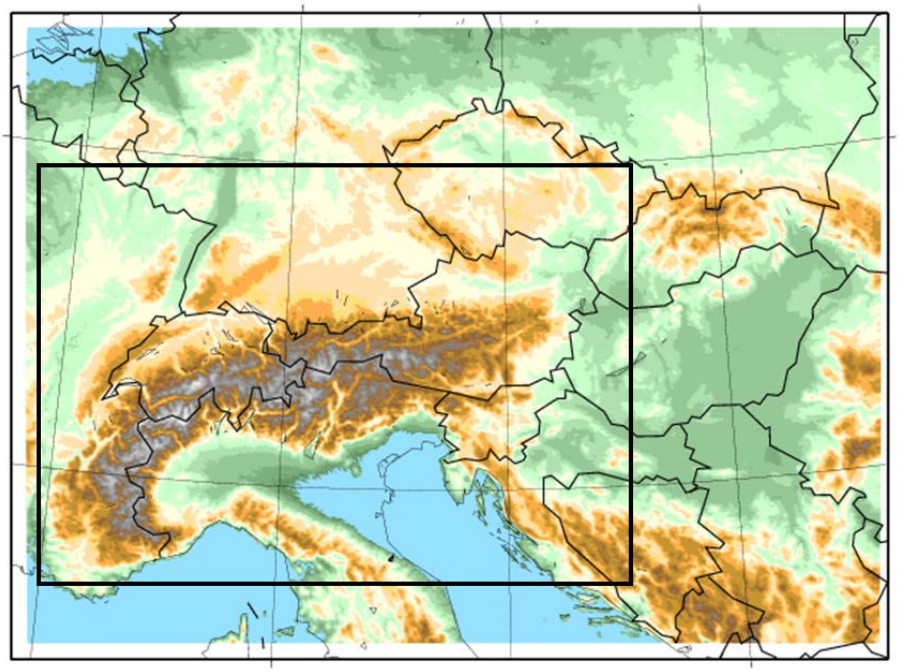

Figure 1: small domain (black line) and big domain

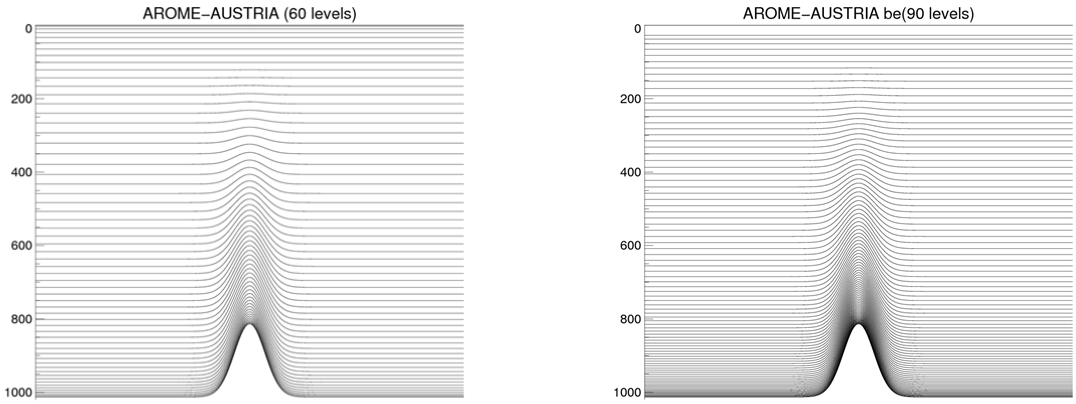

Figure 2: Vertical levels setup for 60 (left)/90 (right) levels

2.2 Observations assimilated inside Austrian AROME/3DVAR

The observations which are assimilated are summarized in the following table. Notice that some observations such as GPS are only assimilated in an experimental mode.

Table 2: Observation assimilated inside AROME/3DVAR system

Observation type	**Assimilated fields**	**Data source**
SYNOP + TAWES	T2m,RH2m,U10m,V10m, Φ	ZAMG + OPLACE
AMDAR (aircraft)	U,V,T	ZAMG + OPLACE
GEOWIND (Sat-wind) MSG3	U,V	OPLACE
TEMP (radio soundings)	U,V,T,Q,Φ	ZAMG + OPLACE

PILOT	U,V	ZAMG
Windprofiler (test)	U,V	ECMWF, MARSARCHIVE/OPLACE
MSG2->MSG3->SEVIRI	WV-radiances	OPLACE
NOAA16/18/19 + MetOp-A-B AMSU-A,-B,MHS,HIRS	radiances	OPLACE
MetOp-A IASI	radiances	OPLACE
ASCAT 10m sea winds	U10m,V10m (25km)	ZAMG/EUMETSAT
GPS (experimental)	Zenith Total Delay (ZTD)	TU Vienna
RADAR (experimental)	Reflectivity	Austrocontrol/CONRAD
Lake surface temperatures (experimental)	TS_WATER in OIMAIN	Hydrological services
MODIS snow cover (experimental)	Snow yes/no	ENVEO-CRYOLAND

3 Case study - Central Europe flash floods 2013

In May and June 2013, Central Europe was facing a period with precipitation exceeding climatological amounts, resulting in soil conditions close to saturation. In the end of May and beginning of June, several days of heavy precipitation finally resulted in an extreme flood event in the Danube down-river region such as e.g. the Wachau (Figure 3). 72h accumulated rainfall reached as high as 225mm in cities like Bad-Ischl.

Figure 3: Flash floods on 7th June 2013, Melk Austria

In general, the local operational model ALARO together with other regional models (like e.g. COSMO) captured the precipitation area quite well and outperformed the global counterparts (ECMWF, GFS). Table 3 shows the area mean precipitation forecasts for four different catchment areas in Austria for various models. The colours indicate to what extent the observed area means where captured by the models. It can be seen that ALARO forecasts are in much better correspondence (and therefore coloured green) with observation (INCA-ANA) than other models. However, some local high peak values (see Fig. 4) were also clearly underestimated by ALARO.

Table 3: Area mean precipitation forecasts for 4 different catchment areas (RR-Zentrum, Einzug Donau, Einzug Inn and Nordstau) for different models and analysis (INCA-ANA).

model init 31.05. 00 UTC
valid 03.06. 00 UTC
period 72 hours
fc type area mean (mm)

	RR-Zentrum	Einzug Donau	Einzug Inn	Nordstau
ALARO5	155,8	90,4	115,9	112,8
ECMWF	120,7	80,3	100,7	90,5
GFS	87,9	74,5	91,3	77,1
COSMO-EU	139,6	77,0	106,9	92,5
EC-EPS *)	81,8	62,5	75,1	69.68
LAEF *)	111,5	80,1	93,3	96,4
AROME **)	-	-	-	-
INCA ANA	146,8	89,4	111,4	112,0

lower limit
130%
120%
110%
100%
90%
80%
70%
60%
50%

*) Ensemble Mean
**) Testbetrieb

24-hour accumulated precipitation map (Figure 5) and precipitation scores (Table 4) within the most affected Salzburg and southern Bavaria region (Figure 4, black framed region) are compared between AROME and the local operational model ALARO5. AROME showed clearly better results in simulating the local rainfall peak values (Figure 5). And the AROME SAL scores outperform ALARO5 for all three aspects (amplitude, structure and location).

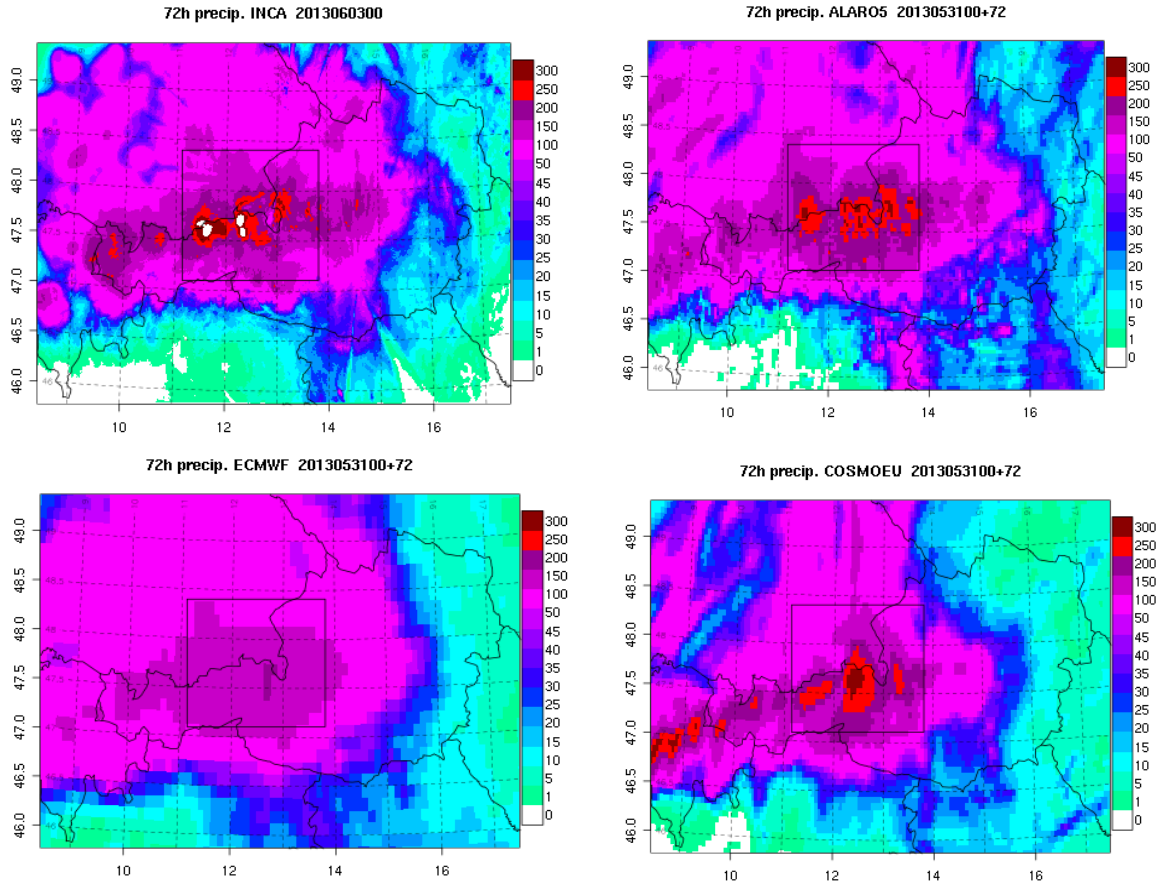

Figure 4: 72h accumulated rainfall between 2013/05/31 00UTC and 2013/06/03 00UTC for (a) INCA analysis (top left), (b) ALARO (top right), ECMWF (bottom left) and COSMO-EU (bottom right)

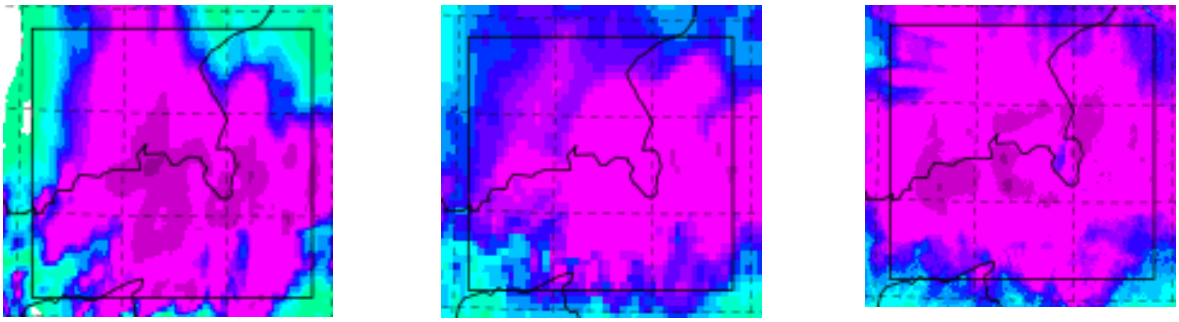

Figure 5: 24h accumulated rainfall between 2013/06/02 00UTC and 2013/06/03 00UTC (left: AROME, middle: ALARO, right: INCA analysis)

Table 4: SAL precipitation scores for 24h area mean rainfall during the three days with strongest precipitation

Model	24h accumulated rainfall (mm)		
	31.5 00UTC – 1.6 00UTC	1.6 00UTC – 2.6 00UTC	2.6 00UTC – 3.6 00UTC
INCA Analysis	33.7	44.5	68.6
AROME	30.5	42.1	63.9
ALARO	23.9	36.8	50.9
SAL (AROME) A/S/L	0.02/-0.10/0.06	0.17/-0.06/0.01	-0.11/-0.07/0.02
SAL (ALARO) A/S/L	0.24/-0.34/0.07	0.32/-0.19/0.01	0.25/-0.30/0.03

4 Additional experiments - GPS assimilation

In cooperation with the Technical University of Vienna, experiments have been conducted to evaluate the benefit of using high density GPS derived humidity data (zenith total delay, ZTD) in the AROME assimilation system. Similar studies have already been carried out in 2010 using a 9.6km ALADIN model version. The results with AROME are more promising and seem to justify an operational usage.

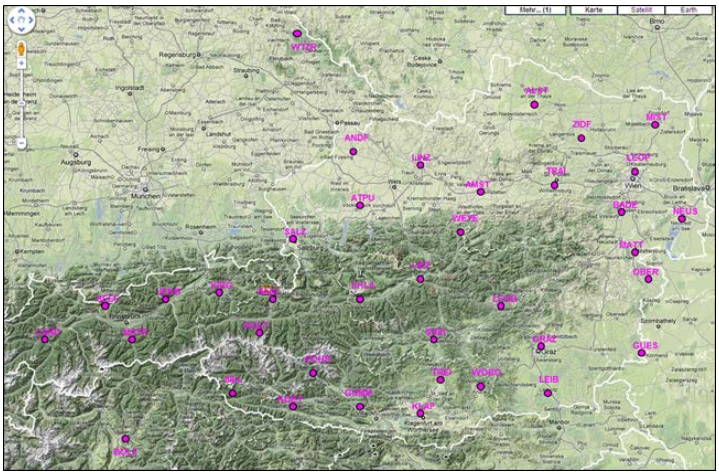

Figure 6: GPS observations used in the additional test experiment

For the test period May - July 2011 the verification shows that using GPS data in the assimilation has a small, but overall positive impact on the scores for the amount, shape and distribution of the simulated precipitation. Figure 7 shows the SAL amplitude and structure scores for the north-eastern Austrian region for a threshold greater than 1.0mm of precipitation. The scores are calculated using 12UTC forecasts up to 30h from May 15th till July 1st, 2011. One can see that experiments with GPS data (red) obtained a better score than experiments without GPS data (blue).

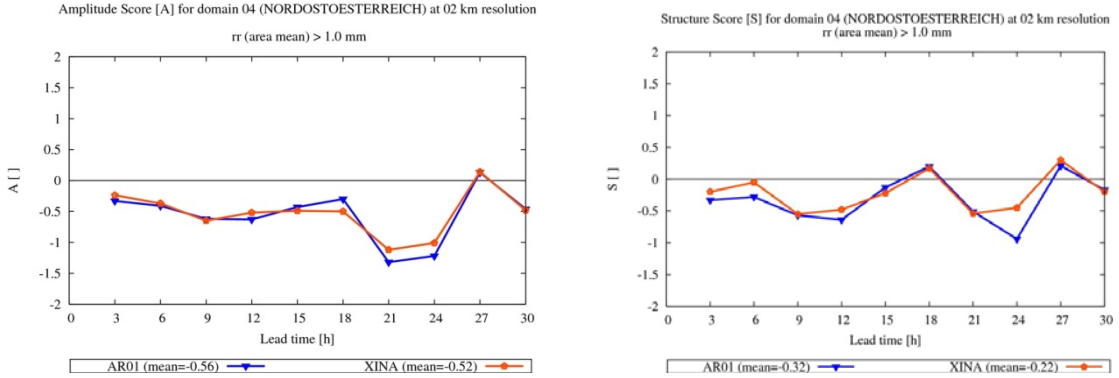

Figure 7: Amplitude (left) and structure (right) SAL scores with (red) and without (blue) GPS ZTD data being assimilated

5 Summary

By the end of 2013 AROME/3DVAR system at ZAMG officially gets an operational status. It is designed to yield more detailed information for users in geographical areas where ECMWF/ALARO5/LAEF show clear deficiencies.

So far the performance of AROME is quite promising, however from time to time it showed some instability for the results. Within the next months several possible operational upgrades of the system are undergoing intensive evaluations to find future optimal set-ups. The tests include: alternative model version and physics options, enlargement of the domain, increase of vertical resolution, increase of coupling frequency, addition of new observation types for assimilation (radar reflectivity and radial wind) and coupling model (IFS vs. ALARO vs. ARPEGE).

For ZAMG, AROME offers a wide range of possibilities to develop new products for users like: Hail diagnostics, lightening diagnostics, simulating radar reflectivity and satellite channels, etc.

Main NWP achievements in 2013 at the Hungarian Meteorological Service

Gergely Bölöni, Dávid Lancz, Máté Mile, Roger Randriamampianina, Balázs Szintai and Mihály Szűcs

1 Introduction

This short article gives an overview of the most important achievements within the NWP group of the Hungarian Meteorological Service (OMSZ) during 2013. Activities within data assimilation, ensemble prediction and physical parametrizations are highlighted, mostly concerning the AROME model using 2.5 km horizontal grid spacing and 60 levels.

2 Data Assimilation

Operational 3DVAR data assimilation for AROME

A 3DVAR data assimilation scheme has been implemented operationally in March, for the AROME model covering the Carpathian basin with its forecasts at 2.5 km horizontal resolution and 60 vertical levels (CY36T1). For the time being only conventional observations (surface stations, radiosonds and AMDAR aircract measurements) are assimilated in a 3-hourly cycling. The surface initial conditions are interpolated from the ALARO operational OI (CANARI at 8 km horizontal resolution) surface analysis at 00, 06, 12 and 18 UTC. In the intermediate analysis times (03, 09, 15 and 21 UTC) an open loop SURFEX forecast provides the surface initial conditions without any assimilation. Tests have been done to apply the OI_MAIN scheme for surface assimilation but so far no added value could be shown compared to the current operational configuration. The introduction of 3DVAR improved the screen level scores (see an example in Fig 1) and reduced the overestimation of the convective precipitation during summer afternoons (Fig 2.) It worth mentioning, that due to the local 3DVAR data assimilation, wind forecasts at ~100 m height have been improved. This improvement allowed to switch to AROME as a basis of specialized wind forecasts given to wind power plants, instead of the “DADA” dynamical downscaling from the hydrostatic ALARO forecasts run at 8 km resolution.

Radar data assimilation

The assimilation of radar data has been a high-priority during the year. Several case studies and periods have been run using the data (reflectivity and radial wind) from the 3 radar sites over Hungary. Objective verification shows a slight improvement in the forecasts of precipitation, however also a slight degradation was found in 2m relative humidity, in case of using all scan heights in the assimilation. Tests were also run using a filtering of the data below 1000 m, which eliminated the 2m relative humidity bias but also decreased the benefit in precipitation. In Fig. 3 a simple case study is shown, where radar assimilation improved the structure of the very short-range precipitation forecast.

3 Ensemble prediction

Experimental AROME EPS

AROME EPS experiments are run with 11 members using CPU resources of an ECMWF Special Project. On the one hand, the experiments were concentrating on the representation of the model error via the application of the Stochastically Perturbed Parameterized Tendencies (SPPT) and on the other hand on the improvement of the initial condition perturbations using an Ensemble Data Assimilation (EDA) approach which was implemented in a frame of a LACE stay. In Fig. 4, a score comparison is shown for the experimental AROME EPS system at 2.5 km resolution (with different settings of SPPT) and the operational ALARO EPS at 8 km resolution over a 2 weeks period (26 December 2011 – 8 January 2012), which shows a likely benefit of using the higher resolution EPS system. The impact of the local EDA perturbations is shown in Fig. 5. This impact is likely to be positive, because an increase of spread and a decrease of RMSE is noticeable for the EDA runs compared to the downscaling of PEARP.

4 Physical parametrizations

Representation of low clouds

An extensive validation of AROME physics took place in order to point out responsible parametrizations for generally poor low-cloud, and related inversion forecasts over the Carpathian basin. These studies have been done in the framework of a bilateral project between Meteo-France and OMSZ. Low-cloud situations with strong surface inversions are typical for Hungary during autumn and winter. Models hardly predict these situations, namely fog and clouds are dissipated much too quickly in model runs, even if the cloudiness is correctly diagnosed in the initial conditions. Besides initial conditions and LBCs, the sensitivity of low-cloud forecasts to turbulence, cloud scheme, and radiation changes was investigated. It has been found that among these, the sensitivity to radiation (optical thickness of clouds) was the largest (see figure 6), but still small to explain the poor forecasts. Recently the role of microphysics schemes have been investigated in low-cloud situations, and results obtained so far show, that this is where changes are more important. Namely, with a relaxation of the auto-conversion scheme, low-clouds remain more persistent in the investigated cases due to the fact that they do not “snow out” too quickly as in the reference (operational) version.

Experiments with AROME at very fine resolution

A PhD work has been started in order to study the effectiveness of the turbulence scheme in AROME if increasing the resolution to the “turbulence grey zone”, i.e. to 1km grid length or below. As a first step a test-bed was set up using a small domain over south-west Hungary (Fig. 7, top panel). Besides the overview of literature, a case study has been run using the test-bed for a convective event (24 June 2013). For this single case, it has been found that precipitation forecasts were not particularly improved by the resolution increase, on the other hand, spurious patterns appeared in the vertical velocity field in the “very fine resolution” test. This gives motivation to run idealized 3D cases with an emphasized focus on the turbulence scheme and its possible adjustments.

5 Summary and Outlook

The above highlighted subjects remain in the focus of our NWP activities in 2014. Additionally surface assimilation experiments using the OI-MAIN and the SEKF schemes are planned as well as a migration of our operational and experimental suites to CY38T1. It is also important to mention that the operational application of the hydrostatic ALADIN (HARMONIE) model using 8 km grid-length, using the ALARO physics package is being continued, both in a deterministic and a probabilistic manner (HUNEPS).

Figures

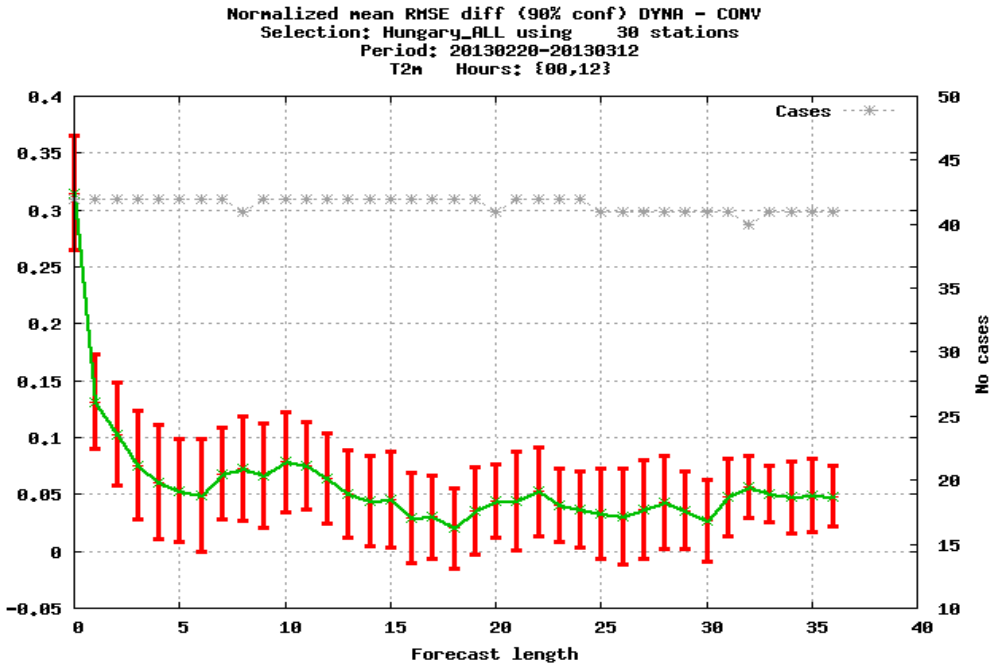

Figure 1: RMSE difference"DYNA – CONV" for T2m, where DYNA stands for "dynamical downscaling" using interpolated ALARO initial conditions and CONV stands for AROME 3DVAR assimilation using conventional observations. The vertical bars show the significance of the RMSE differences using a T-probe with 90% confidence level.

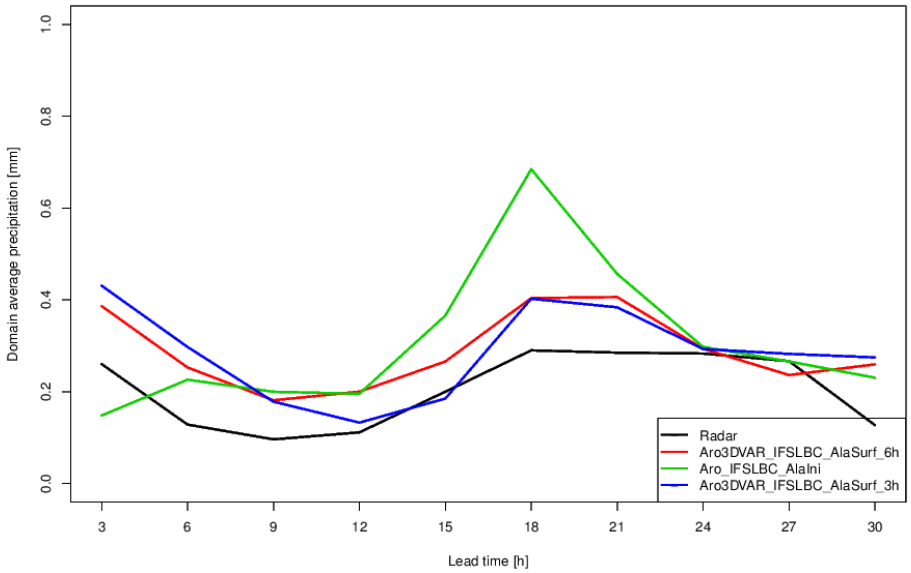

Figure 2: Domain average precipitation statistics for the period 20/06 – 25/07/2012. Black: Radar, Green:AROME dynamical downscaling, Red: AROME with 3DVAR with a 6-hourly cycling, Blue: AROME with 3DAR with a 3-hourly cycling.

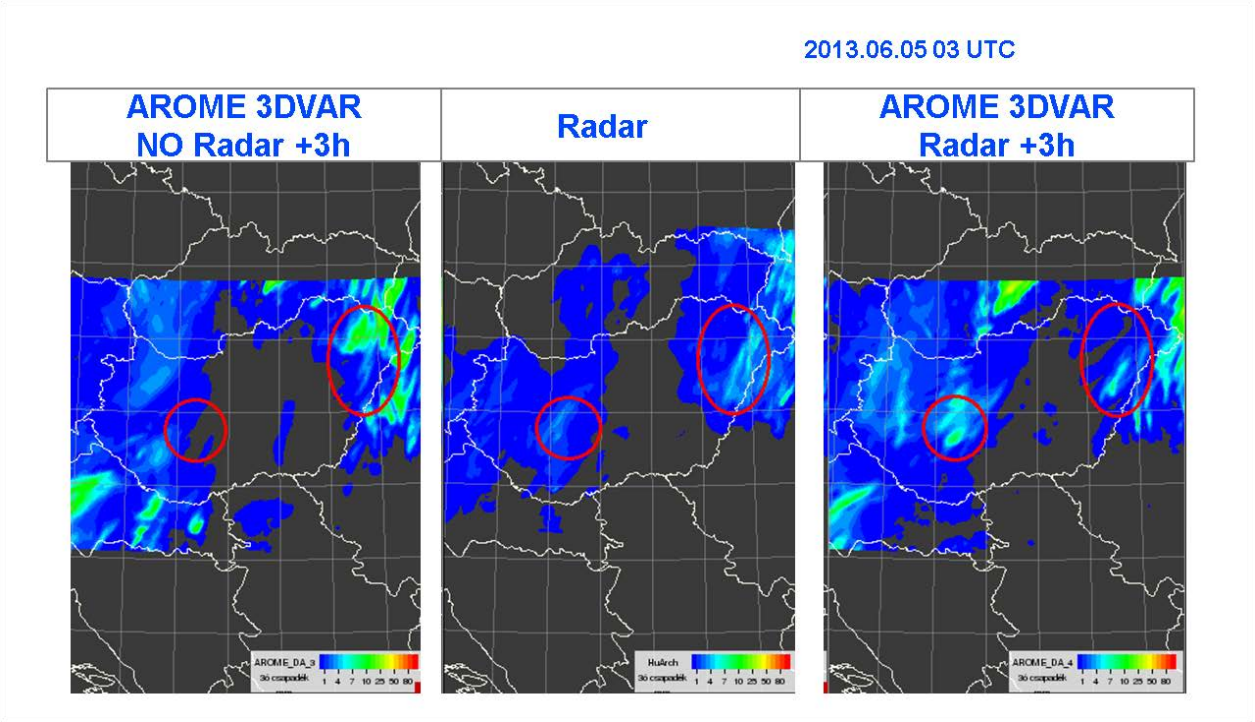

Figure 3: A case study showing the benefits of radar assimilation. Left: precipitation forecast based on AROME 3DVAR without radar assimilation, Middle: radar measurements, Right: precipitation forecast based on AROME 3DVAR with radar assimilation

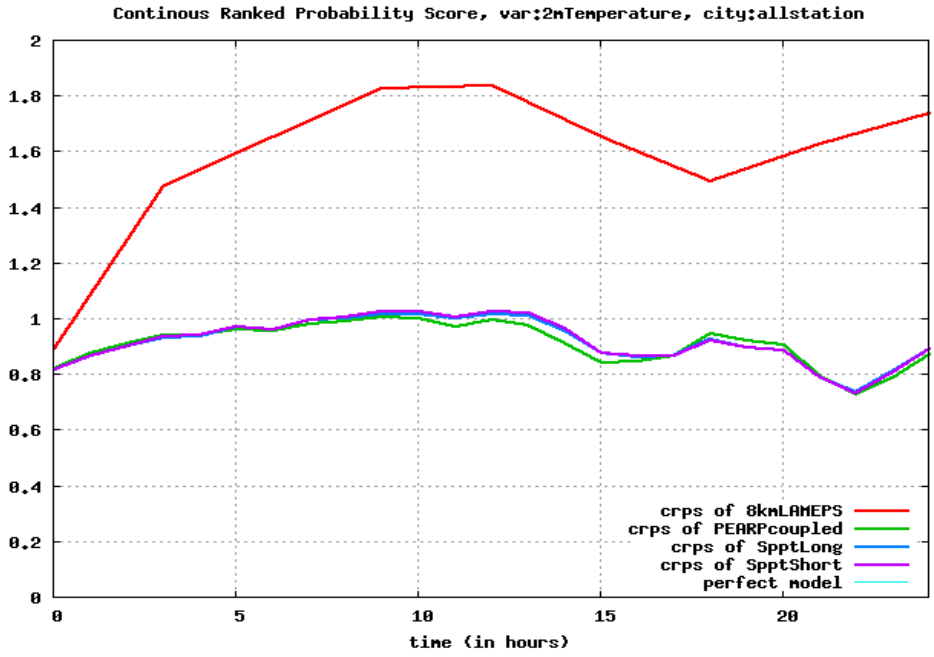

Figure 4: CRPS scores as a function of forecast range, computed for the operational ALARO EPS system (red curve) and the experimental AROME EPS system with different SPPT flavours (green, magenta, blue), over a 2weeks period (26 December 2011 – 8 January 2012)

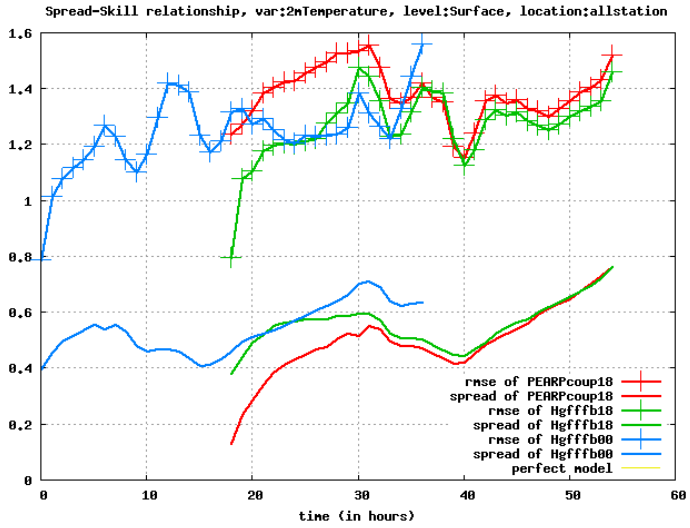

Figure 5: Spread-skill scores as a function of forecast range, computed for the experimental 18 UTC AROME EPS runs downscaled from PEARP (red curve), the experimental 18 UTC AROME EPS runs using local EDA perturbations and PEARP LBCs (green curve) and the experimental 00 UTC AROME EPS runs using local EDA perturbations. Period: 26 December 2011 – 8 January 2012

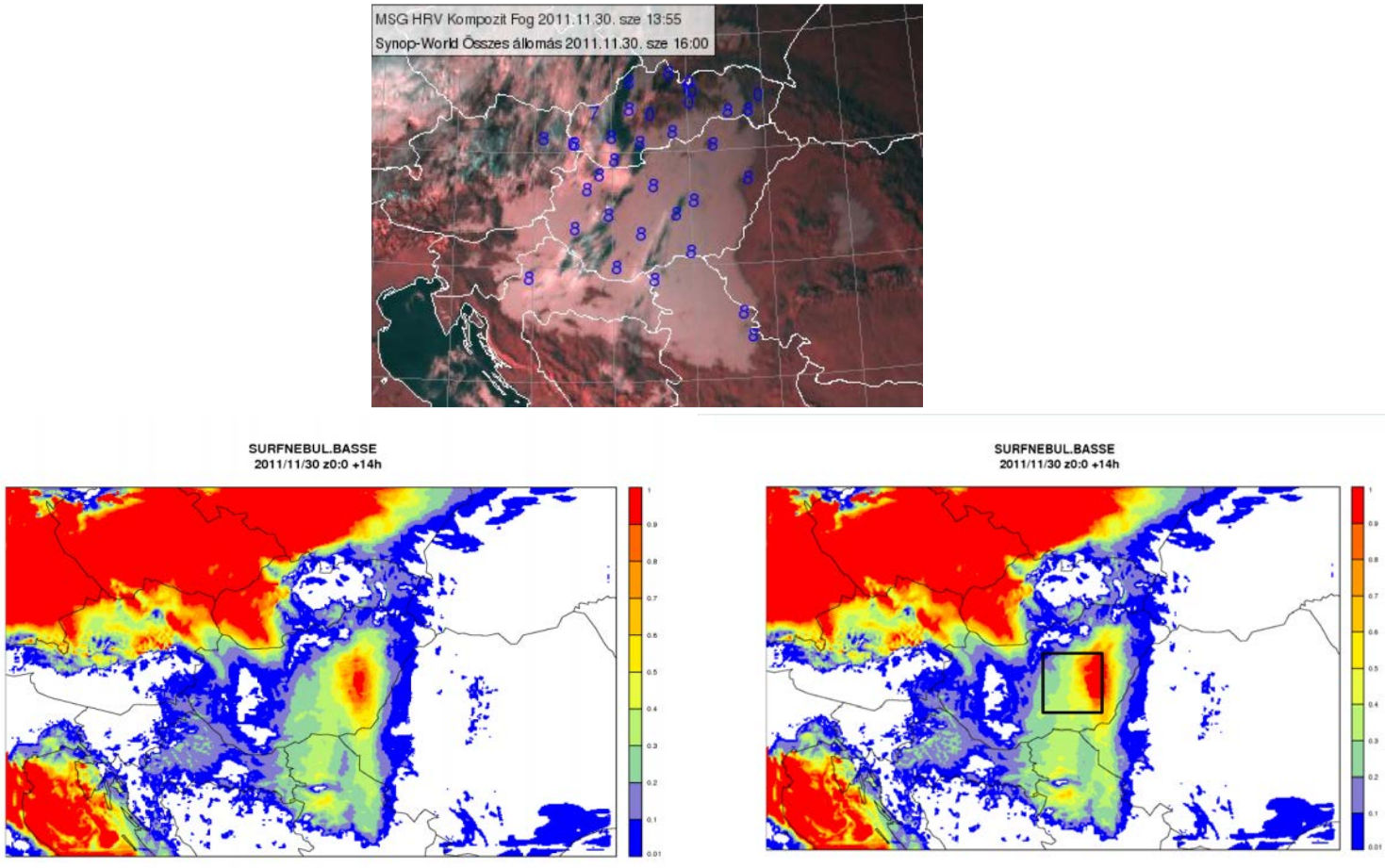

Figure 6: A case study to demonstrate the sensitivity of
Top: Cloudiness as observed from surface stations and from MSG-HRV, Bottom left: AROME cloudiness forecast with operational settings (lower optical thickness RLWINHF =0.7), Bottom right: AROME cloudiness forecast with a new, higher setting of optical thickness(RLWINHF=1.0)

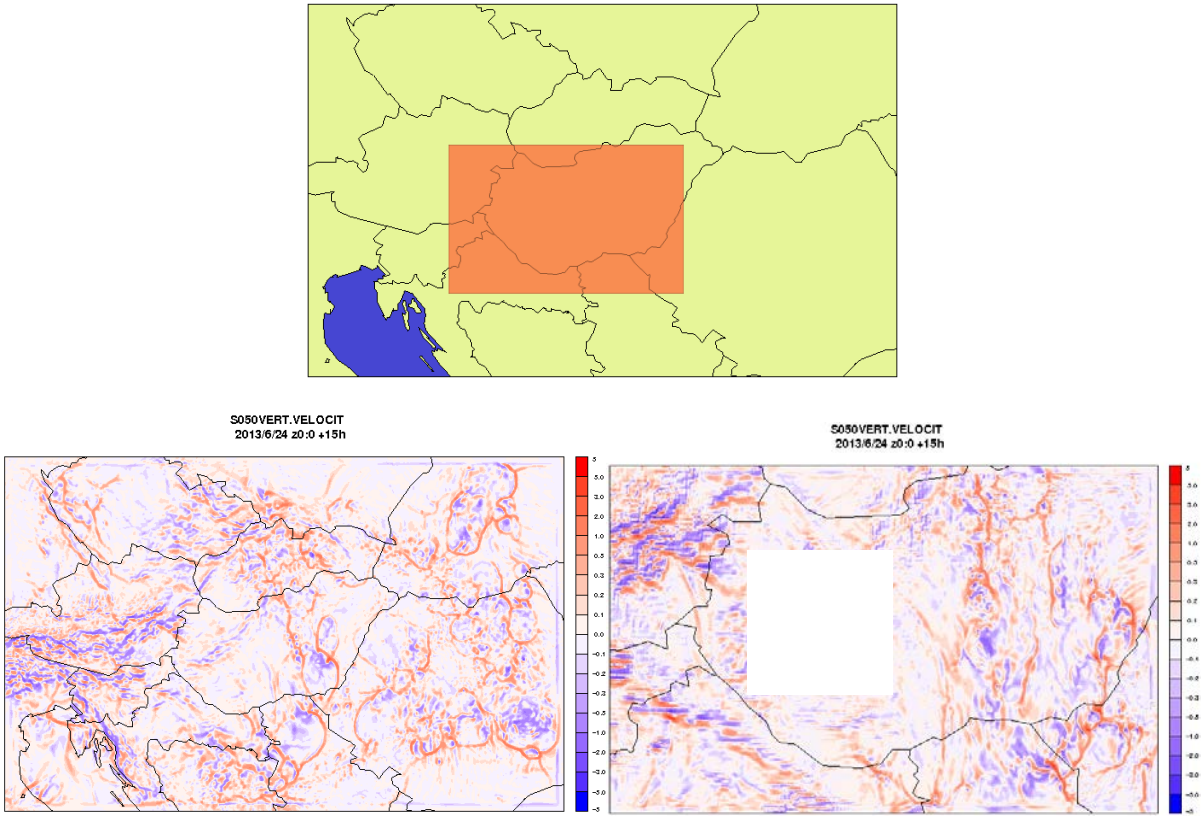

Figure 7: AROME experiments using 1km grid-length. Top: the domain of the 1 km test-bed, Bottom-left: Vertical velocity forecast of the operational AROME model using 2.5 km grid-length, Bottom-right: Vertical velocity forecast of the experimental AROME version using 1 km grid-length, where the black rectangle highlights noisy patterns in the vertical velocity field.

ALADIN and AROME at the DIRECTION DE LA METEOROLGIE NATIONALE of MOROCCO

1 GPS data Assimilation In ALADIN-MAROC

In order to in order to predict as accurately as possible the weather over Morocco, Meteorological service of Morocco have installed a network of 10 GPS stations serving weather needs. Data from these stations are processed locally using the BERNESE software to calculate ZTD (Zenith Total Dealy). The impact of GPS Zenith Total Delay (ZTD) measurements on mesoscale weather forecasts is studied. GPS observations from a permanent Moroccan network are assimilated into the ALADIN-MAROC using its three-dimensional variational assimilation (3DVAR) system.

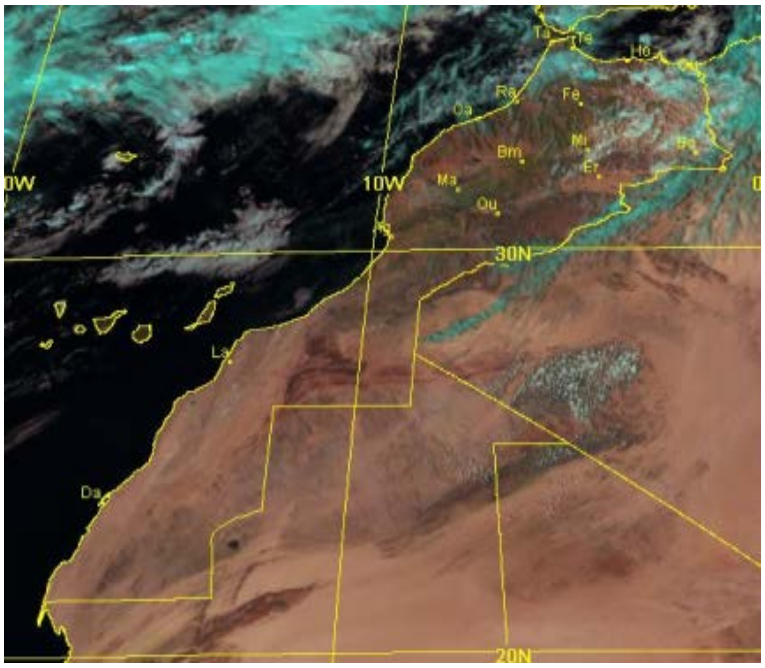

Figure 1: Network of Moroccan GPS stations

The impact is significant concerning relative humidity on several vertical levels (Figure 2).

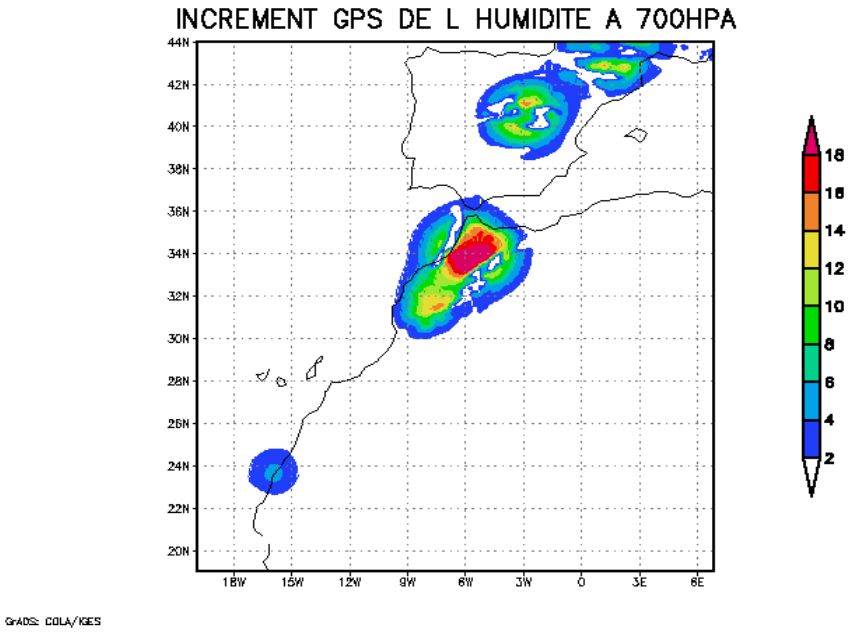

Figure 2: Increments of humidity 700hpa for 28/03/2013 at 00 UTC

2 Installation of cy38t1 in Morocco

The cycle CY38t1 has been compiled and implemented in the double suite. Before its implementation in operation, scores and comparison to cy36t1 have been calculated for both ALADIN-MAROC and AROME MAROC.

In case of ALADIN-MAROC, we can see that T2m and H2m (which was in operational ALADIN model in CY36t1_op1) underestimated the temperature and humidity and that reduces this bias for temperature.

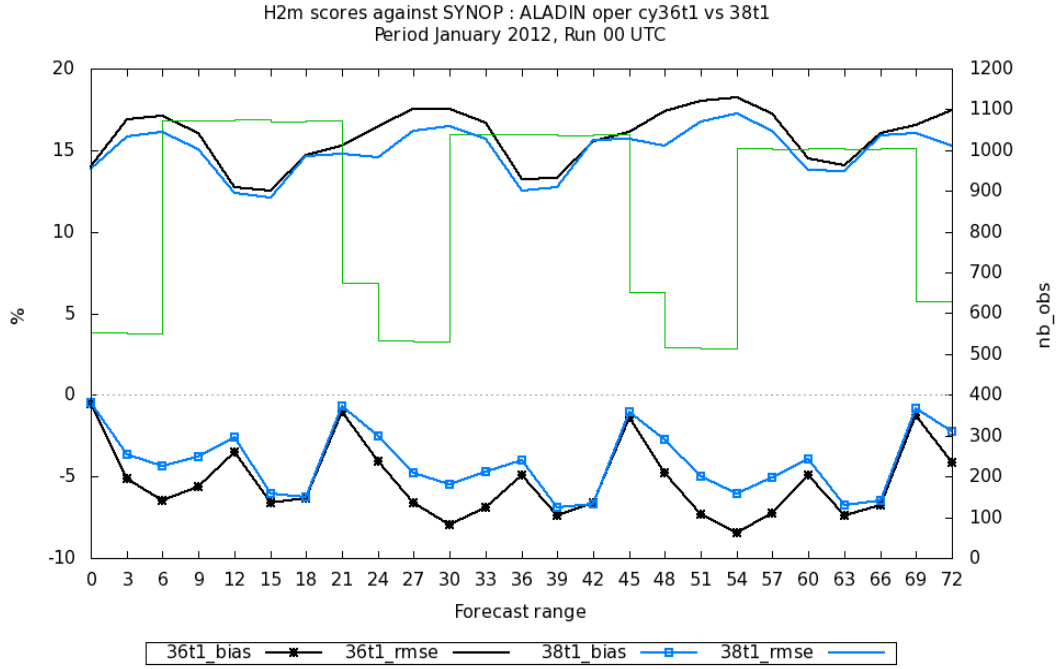
H2m scores against SYNOP : ALADIN oper cy36t1 vs 38t1
Period January 2012, Run 00 UTC
%
nb_obs
Forecast range
36t1_bias
36t1_rmse
38t1_bias
38t1_rmse

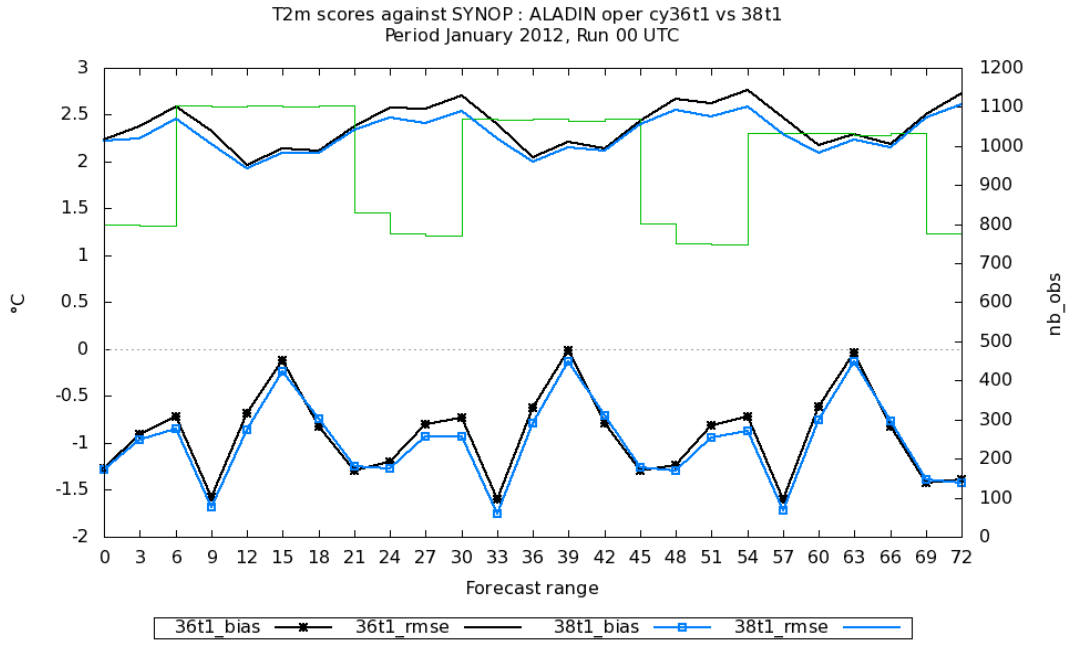
T2m scores against SYNOP : ALADIN oper cy36t1 vs 38t1
Period January 2012, Run 00 UTC
°C
nb_obs
Forecast range
36t1_bias
36t1_rmse
38t1_bias
38t1_rmse

In case of AROME-MAROC the scores show more improvement for temperature than humidity.

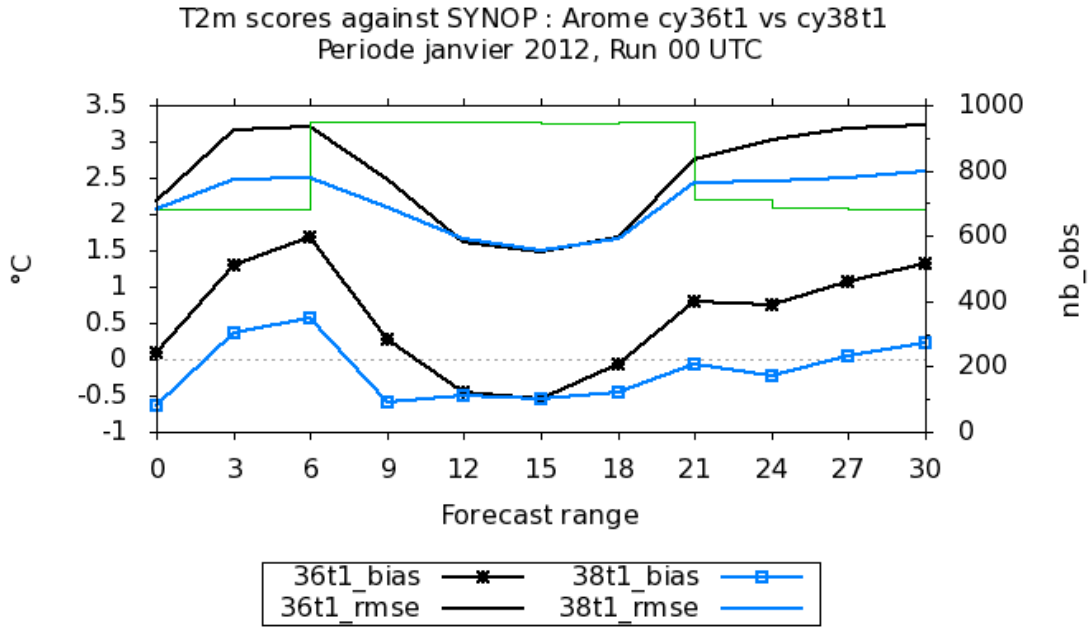

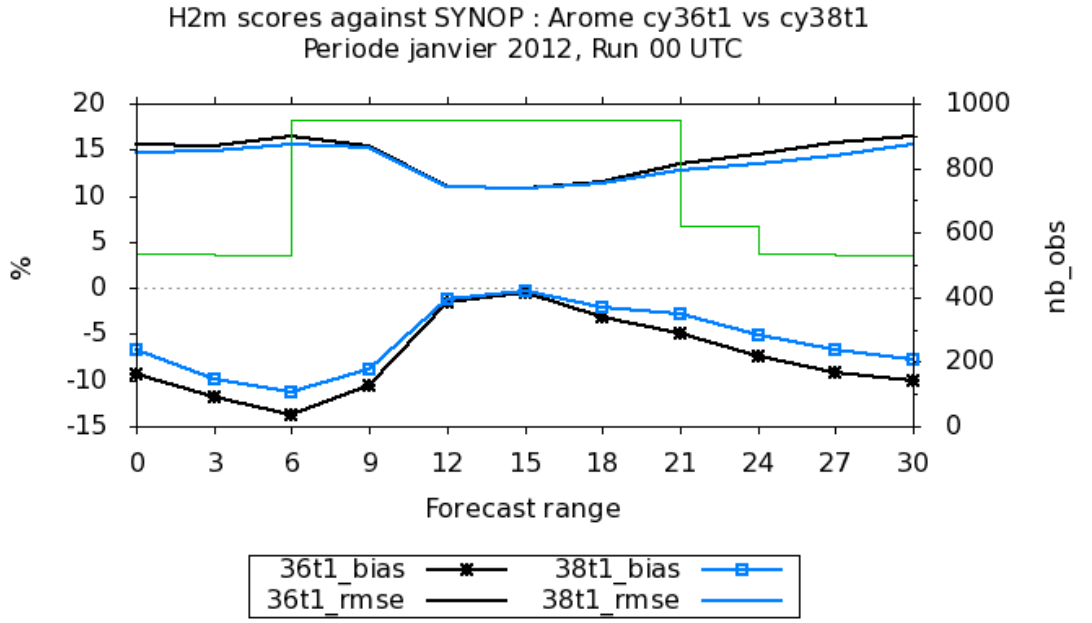

ALADIN in Poland - 2013

Marek Jerczynski, Bogdan Bochenek, Marcin Kolonko,
Malgorzata Szczech-Gajewska, Jadwiga Woyciechowska
Institute of Meteorology and Water Management / POLAND

1 Introduction

In 2013 year the activities of ALADIN team in Poland were mainly focused on the development of wavelet-based verification system, preparation of the wide palette of new visualisation products and testing of ALADIN/ALARO model on newly purchased computational cluster.

2 Description

During last several months wavelet-based verification system was developed at IMWM. Motivation for the work was recognition of the potential of multi-scale attitude for high-resolution forecast verification. The core of the developed system is written in R language and uses SpatialVx package, control and data aquisition software is written in shell and Python languages. WWW interface is built with HTML and JavaScript. Current version of the system enables verification of precipitation forecast against synoptic and automatic measurement stations data. Presentation of results comprises tables of IS Skill Score, Energy and MSE for the sets of given thresholds and spatial scales – see Figure 1.

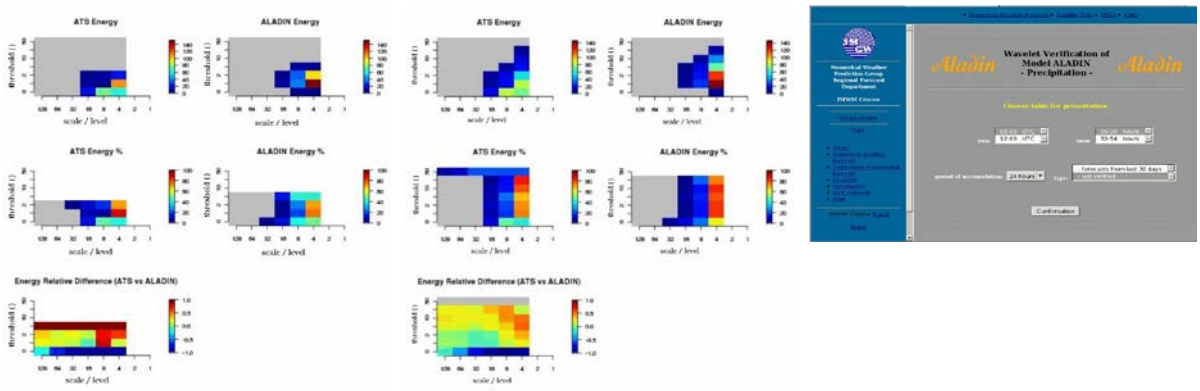

Figure 1: Verification system - examples of available verification products and www interface

Several new operational forecast products were prepared and put into operational usage at IMWM in last several months. Among them new meteograms and maps of severe weather indices: K-Index, Total-Totals, SWEAT, CAPE, SRH, EHI, wind shear. Meteograms are being drawn with R-package called meteogRam (package created by Bogdan Bochenek) and maps with NCARG-NCL software. These forecast products are available in IMWM intranet, examples of them are shown at Figure 2.

Another major work made the period were tests of ALADIN/ALARO model on available computational cluster. The cluster consists of 96 nodes connected with an Infiniband network. Each diskless node comprises two 8-core Intel Xeon E5 – 2690 processors and 32GB RAM. Forecast production performance, scalability and robustness were checked.

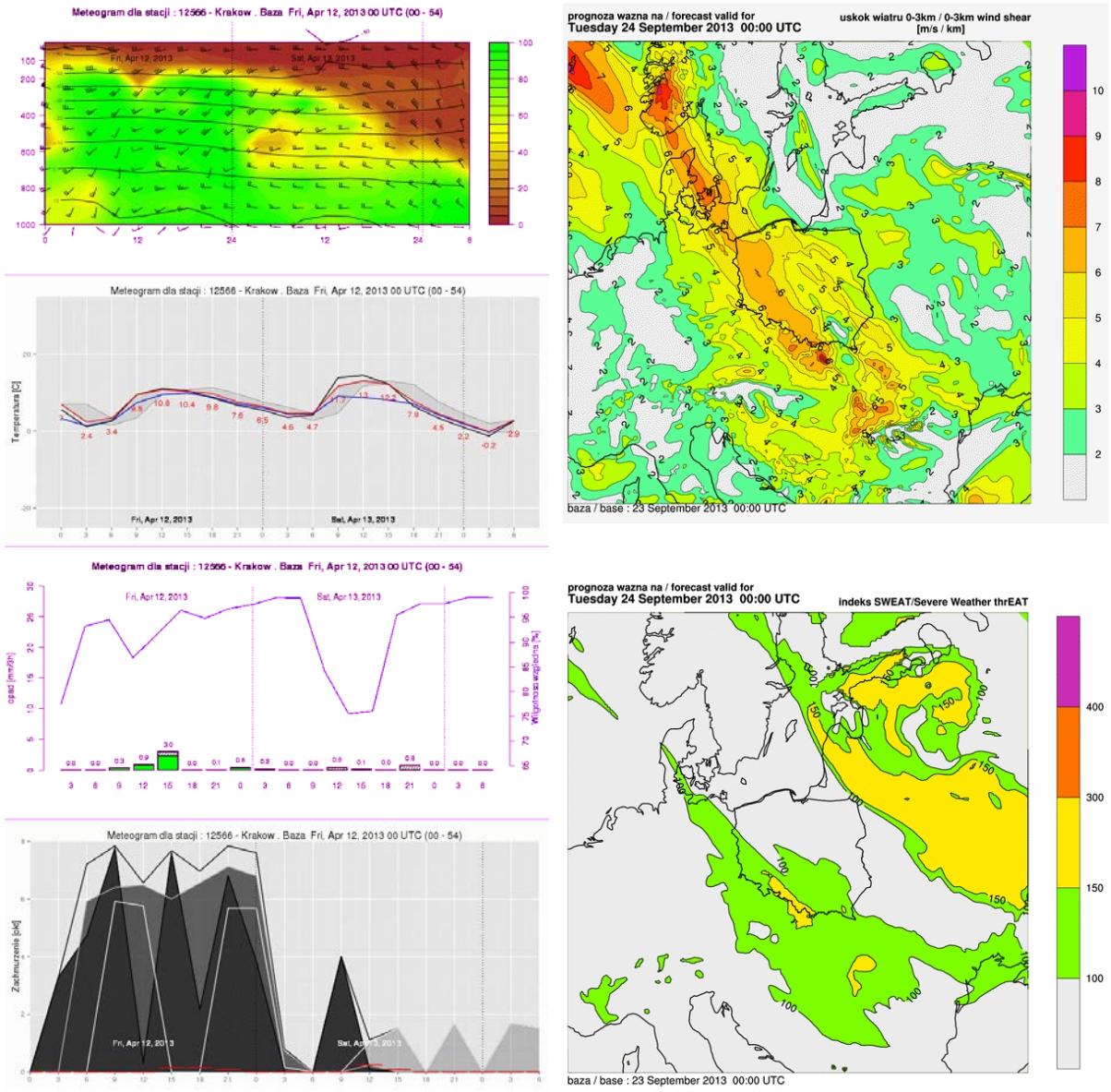

Figure 2: Examples of new operational forecast products

ALADIN Highlights for IPMA, I.P. (Portugal)

Maria Monteiro, João Rio, Nuno Moreira

April 22, 2014

1 Introduction

During last year, main efforts were focused to support the internal and external customers of the NWP products. In particular, the primary focus of these efforts have been on developing new applications based on the ALADIN and AROME forecasts.

In this publication, we highlight one application that has been used regularly by the local forecasting center since 2012. It is the local Spatial Indicator of the Probability of Occurrence of Strong Events (SIPOSE) as we describe below.

2 The local Spatial Indicator of the Probability of Occurrence of Strong Events

For its daily routine, ECMWF, ALADIN and AROME are the main NWP model products in use at the forecasting center, with ECMWF being the reference model when meteorological warnings for extreme events have to be issued. Despite the high horizontal resolution of ECMWF forecasts, it is still too coarse for the detail required nowadays, which can be provided by ALADIN and the convective-scale AROME model. In order to optimise the available information provided by the different models at the forecasting center and in order to support the decision process of the forecaster, a new forecasting product has been created, using the already available numerical products from ECMWF dissemination and the run of local models.

Conceptually, the SIPOSE can be seen as a simplified version of a multi-model lagged ensemble. Its 6 members are provided by the operational run of the deterministic ECMWF, ALADIN-Portugal and AROME-PTG models. In this ensemble, 00UTC and 12UTC products up to the range of 48 hours, with a time-step of 3 hours, are used at their original horizontal resolutions. SIPOSE products are available every 3 hours at a choosen horizontal resolution of 0.25 degrees. On each product range it is assumed that the different members are not mutually correlated, which means that they simulate the same event in a complete independent way, with the same probability.

For the time being, SIPOSE is used as a spatial indicator of the probability of occurrence of strong events of wind intensity, gust and precipitation above pre-defined thresholds. The values of 1mm/3h, 10mm/3h and 20mm/3h are used as limits for the precipitation; for the wind intensity the values of 10m/s, 15m/s and 20m/s are used while for gust the values of 15m/s, 20m/s and 25m/s are considered as threshold.

As an illustration, the Figure 1 shows the location of the averaged spatial probability of accumulated precipitation occurrence for the range of 36 hours on the domain of AROME-PTG, valid at 12UTC on 27 September 2013. The different panels in this illustration show the spatial probability above the different pre-defined limits.

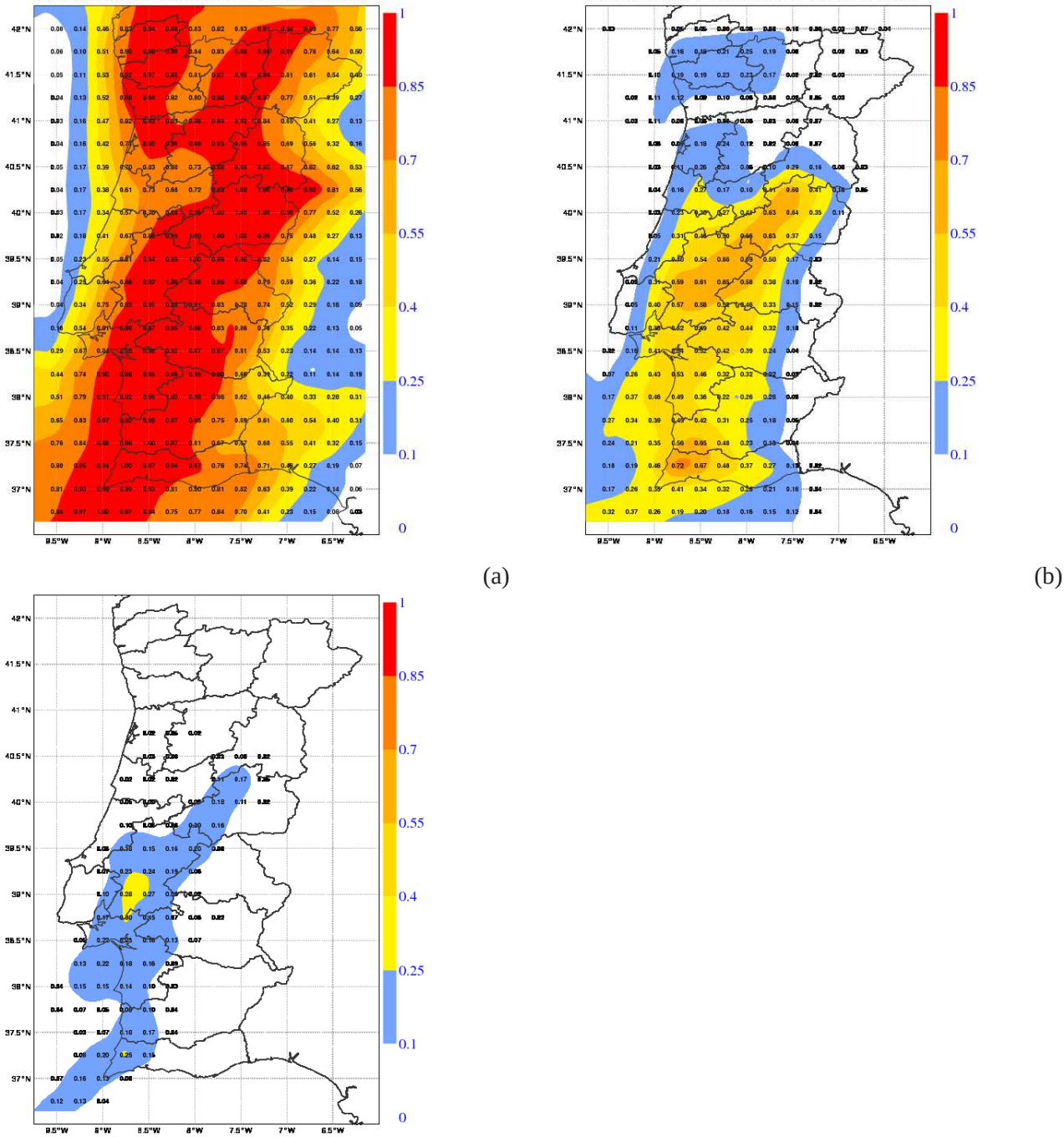

Figure 1: Spatial indicator of the probability of occurrence of precipitation events, valid at 12UTC of 27 September 2013, for different thresholds: (a) 1mm/3h, (b) 10mm/3h and (c) 20mm/3h.

It tells, in an objective and concise way, how consistent is the forecast information between the three models (shown in panels of Figure 2), when an active cold front is forecasted over Portugal mainland (see Figure 3).

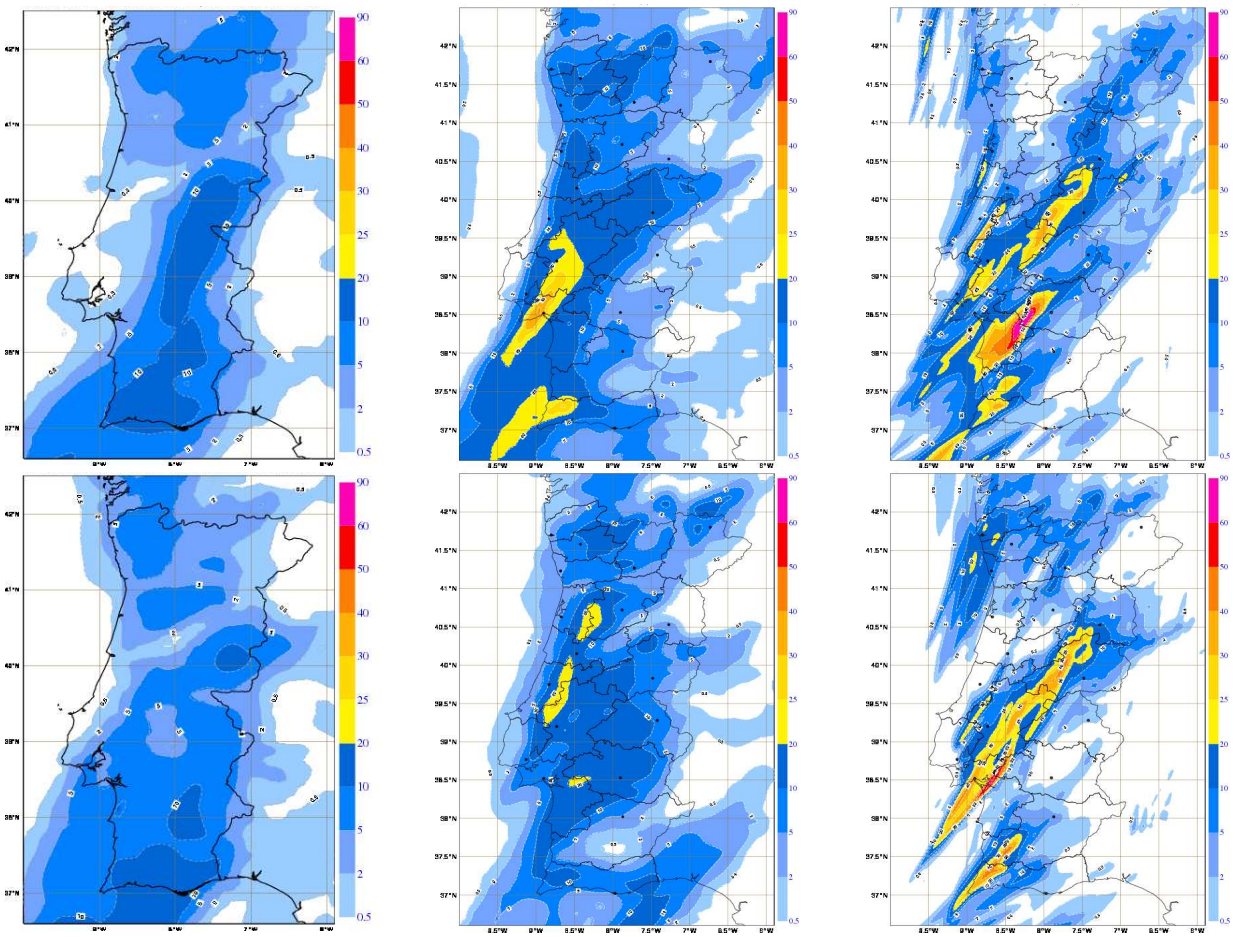

Figure 2: Accumulated precipitaton forecast valid at 12UTC on 27 September 2013, for the models of ECMWF (left), ALADIN-Portugal (middle) and AROME-PTG (right) and for the ranges: 33-36 (top) and 48-45 (bottom).

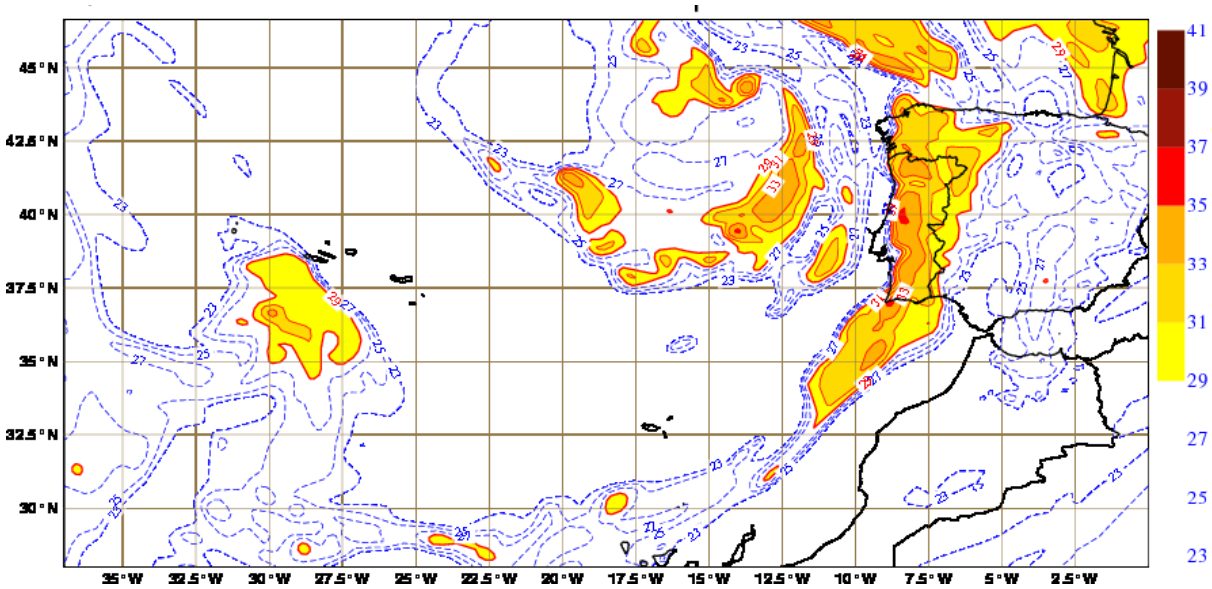

Figure 3: ALADIN-Portugal forecasted Jefferson stability index calculated for a 36 hour range, valid at 12UTC for 27 September 2013. Unit: °C.

References

Rio J., Implementação de um sistema de previsão probabilista com base nos modelos numéricos operacionais no IM, I.P., Nota Técnica 04/2011, DMC/CPPN, IM,I.P., dez 2011.

ALADIN related activities @SHMU (2013)

Mária Derková, Jozef Vivoda, Martin Belluš

1 Introduction

The summary of ALADIN related activities at Slovak Hydrometeorological Institute in 2013 is given. The setup of ALADIN operational system is described and two research activities performed within RC LACE collaboration are highlighted.

2 Operational ALADIN/SHMU NWP system

The ALADIN/SHMU operational setup

The operational ALADIN/SHMU NWP system covers so-called LACE domain with 9km horizontal resolution and 37 vertical levels. It is operated on IBM p755 HPC platform since May 2011, 4 times per day up to +72h. Current model version is based on CY36T1 with so-called ALARO+3MT physics and ISBA surface scheme, coupled to Arpege global model. The spectral blending by digital filter is applied for the upper-air pseudo-assimilation using Arpege analysis. The CANARI surface data assimilation scheme using additional local observations is active since April 2012. More ALADIN/SHMU details are given in Table 1.

Table 1: ***ALADIN/SHMU - operational computer and model***

Model version	ALADIN/ALARO, CY36T1_bf10
Resolution	9.0 km
Levels	37
Area	2882 x 2594 km (320 x 288 points) [2.19 ; 33.99 SW] [39.06 ; 55.63 NE]
Initial conditions	CANARI surface analysis & upper-air spectral blending by DFI 6 hours cycling
Boundaries	ARPEGE, 3h coupling frequency
Starting times	00, 06, 12, 18 UTC
Forecast length	+72h (+60h at 18UTC)
Physics	ALARO+3MT
Surface scheme	ISBA
Dynamics	2TL SL hydrostatic; SLHD
HPC	10 nodes of IBM Power 755: 4x Power7 8core CPUs, 256 GB RAM total: 320 CPUs, 2.5 TB RAM
Management servers	2x IBM Power 750: 1x Power7 6core CPU (3.6 GHz), 64 GB RAM
Software & file system	AIX 6 SE OS, IBM Load Leveler queueing system, 40 TB GPFS

Activities in Y2013 and plans for Y2014

In 2013 the tuning of diagnostic cloudiness based on the near maximum overlap of adjacent layers [after Wittmann, 2009] has been performed in order to cure the syndrome observed in the operational setup when cloudiness rarely exceeded 70-80%, even in case of long lasting frontal precipitation. Improvement in terms of verification scores and in more realistic and nice-looking cloudiness pictures has been noticed.

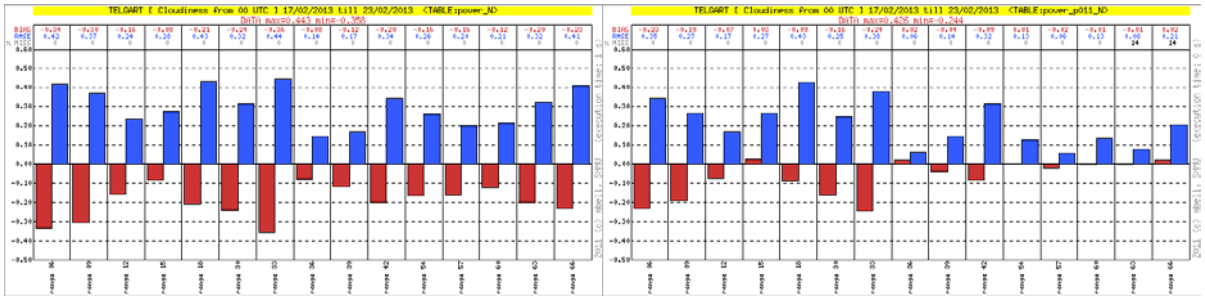

Figure 1: Example of the station verification for one week of the parallel suite with modified cloudiness. Former setup on the left, the one with improved cloudiness on the right.

The porting and extensive validation of CY38T1_bf03 has been performed including full ALARO-0 physics setup with rather positive results (see Fig. 2). However, the spin-up observed in tested version at the beginning of integration shall be understood and eliminated.

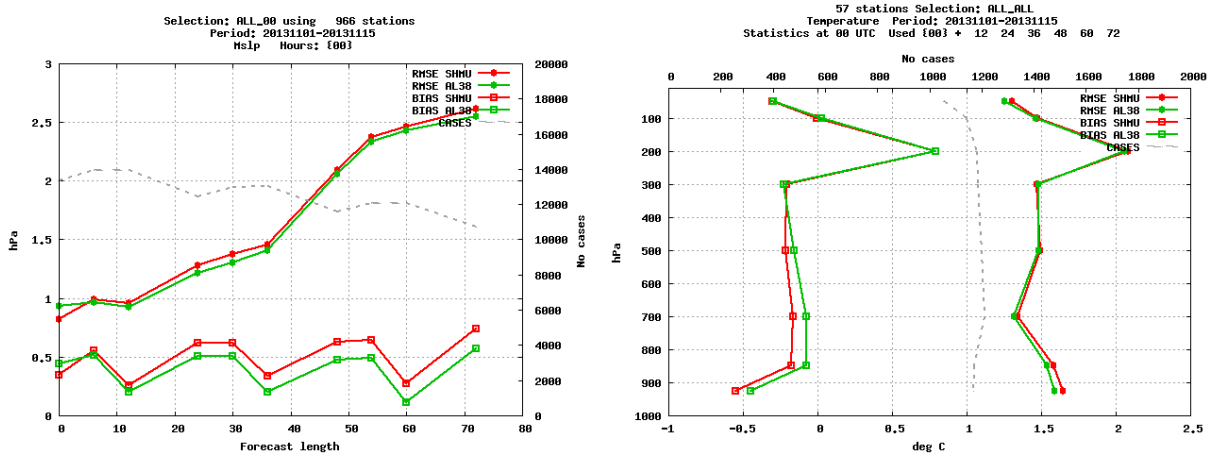

Figure 2: Example of verification results of the parallel suite with CY38T1_bf03 (green) versus the operational scores (red).

It is planned that CY38T1_bf03 will be operationally implemented early in 2014. Consequently, the tests with increased of horizontal and vertical resolutions will be resumed.

3 Research and Development activities

Finite element vertical discretization for ALADIN non-hydrostatic dynamics (J. Vivoda)

FE vertical discretization has been extended from hydrostatic to non-hydrostatic dynamics: prognostic quantities interpolation using B-spline curves was constructed with de Boor's recursive algorithm. The treatment of boundary conditions was modified and the stationary iterative solution of the Helmholtz structure equation was implemented. Set of idealized tests was performed proving satisfactory

accuracy and stability properties of proposed finite elements scheme. A dedicated article (Smolikova and Vivoda, 2013) has been published in previous ALADIN-HIRLAM Newsletter.
The work has continued in the second half of 2013 in form of RC-LACE stay in Prague, in cooperation with P. Smolikova (CHMI), A. Subias and J. Simmaro (AEMET), and on coding issues with K. Yessad (Meteo-France). The stay was dedicated to cleaning of existing code and phasing the development made on cy36t1 into cy40. The following topics were covered:

- The definition of eta levels in the maximas of splines;
- The definition of knots from the predefined full levels (the splines have maximas close to full levels for computed knots sequence);
- The definition of invertible operators (derivative and integral) (LVFE_FIX_ORDER);
- The implementation of invertible operators into the model (LVFE_GW key) with gw on model full levels;
- The implementation of invertible operators into the model (LFE_GW_HALF) with gw on model half levels;
- A cleaning of the code and its optimization;
- 3D idealized tests (1km resolution ALP domain);
- 2D idealized tests;
- The study of pure VFE definition of laplacian operator (up to now we are obliged to use top boundary condition (TBC) and bottom boundary condition (BBC) in VFE manner).

A complete report from the stay will be available on the RC LACE web pages (www.rclace.eu).

ALADIN-LAEF (Martin Bellus)

The development of ALADIN-LAEF configuration within RC LACE cooperation has continued. Three main topics were tackled during 2013:

- The study of different coupling strategies and their impact on the LAEF scores and overall performance;
- The sensitivity tests with the size of the LAEF ensemble;
- The verification of new ALADIN-LAEF setup and an upgrade of the verification package.

Time Consistent versus Space Consistent coupling – what is the impact?

Space Consistent Coupling (SCC) denotes such experiment setup where the very first coupling file (LBC0) is identical with the initial file (that comes e.g. from assimilation procedure). Other LBC files are provided by driving model. The data in the coupling zone in the very first time step are consistent in space, but between LBC0 and LBC1 they are inconsistent in time. On the contrary, in Time Consistent Coupling (TCC) experiment setup, all lateral boundary tendencies are coming from the driving model. But the data in the coupling zone are inconsistent in space. No differences between TCC and SCC setups are visible at 00 range (obvious). In subsequent timesteps the signal propagates from the boundaries inside the domain (Figure 3), with bigger amplitudes in weather-active areas (e.g. frontal zones: Figures 3 and 4). However, no impact is seen on long range verification scores over whole domain (Figure 5). This opens a scientific question whether the method can be used to create targeted LAM perturbations?

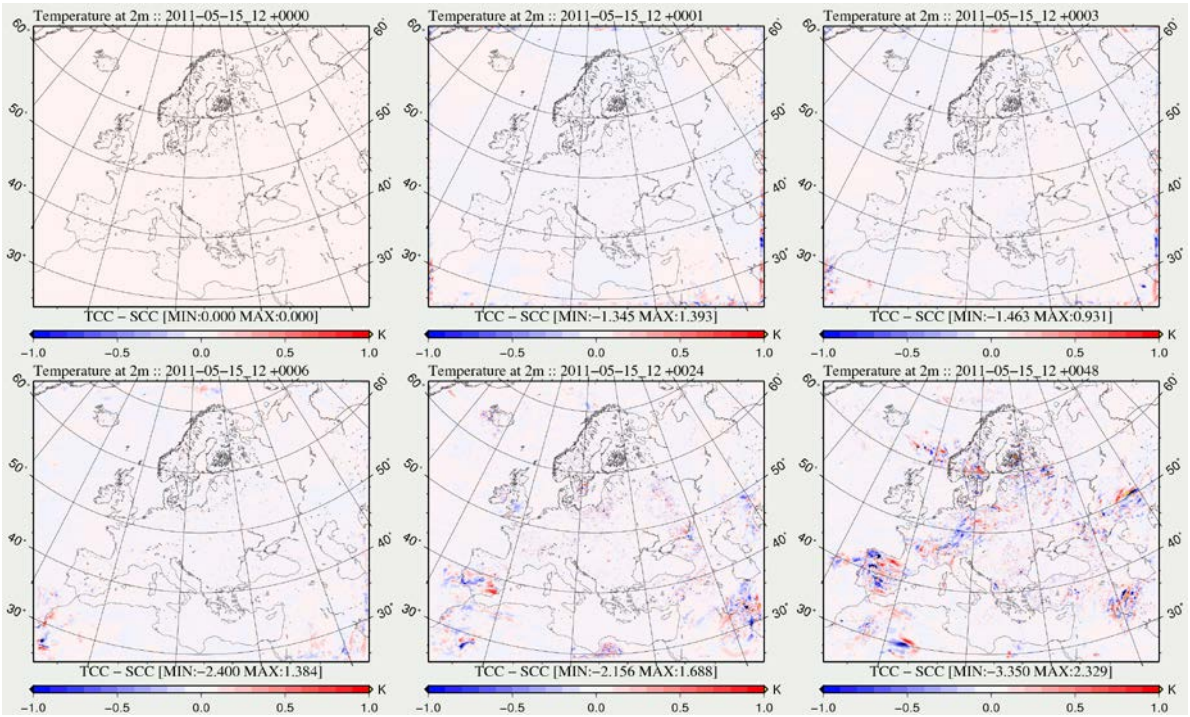

Figure 3: The differences in 2m temperature forecasts between TCC and SCC methods for selected forecast ranges.

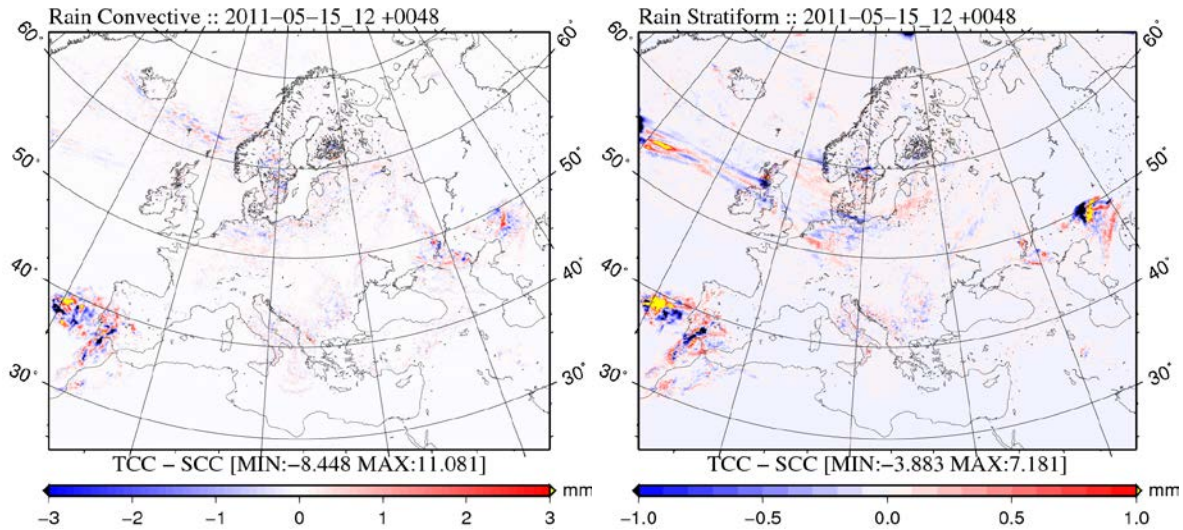

Figure 4: The differences of 48h precipitation forecast between TCC and SCC methods.

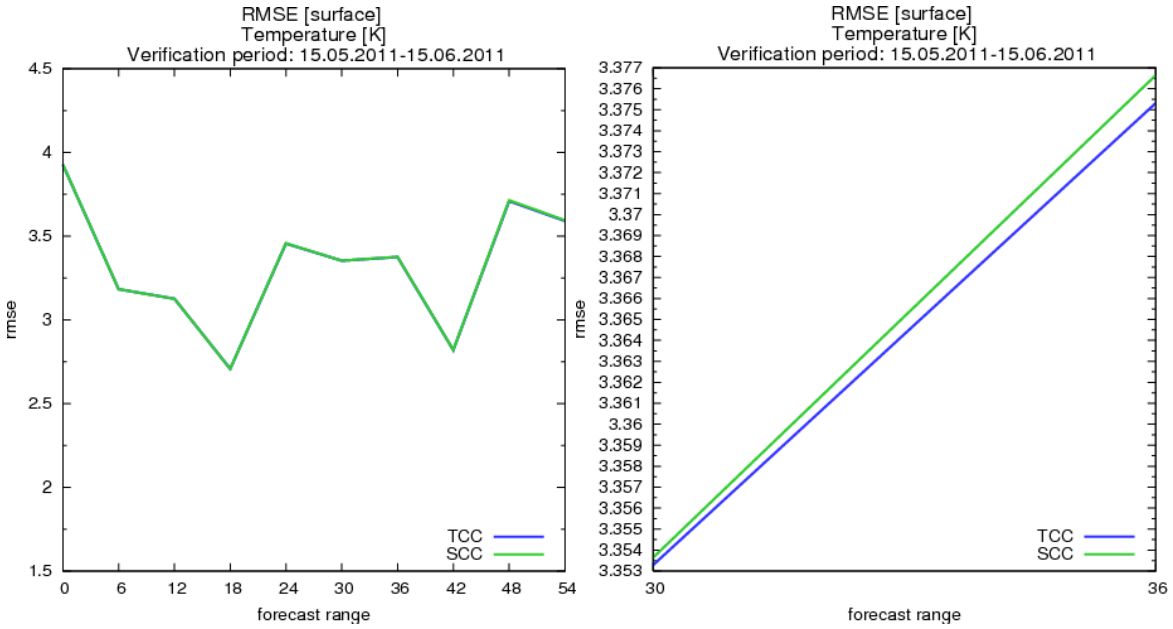

Figure 5: The RMSE of 2m temperature for TCC and SCC methods; with zoom for the +30 and +36h ranges on the right.

The sensitivity tests with the size of the LAEF ensemble

The two experiments coupled with 50 ECMWF global members were done in order to verify the value of ensemble size for LAM EPS: 1) ALADIN-LAEF without multiphysics (but with 12h upper-air and surface pressure breeding, surface assimilation of perturbed T2m and RH2m observations and upper-air spectral blending for the initial conditions); and 2) ALADIN-LAEF with multiphysics, where 10 selected e001 namelists for different physical parameterizations and model tunings were repeated for all 50 members using the key 01-10, 11-20, 21-30, 31-40, 41-50. Subsequently the ensembles consisting of subsets counting first 10, 20, 30, 40 and all 50 members were verified and compared to each other. The first results from one month of integration (June 2011) are shown. To warm up the surface assimilation cycle with the perturbed observations, a 20 day's integration up to +12h was also carried out starting at 11th of May 2011.

The preliminary verification scores showed that the biggest difference is between 10-member and 20-member ensembles, while for the higher member counts the system seems to be already saturated. This can be applied equally to both experiments - without multiphysics (the effect of boundary conditions only) and with multiphysics (LAM model uncertainty included). While the scores for the EPS means are almost independent on the ensemble size, in the second experiment, the clustering of members by multiphysics is obvious (can be seen in BIAS charts for instance, but not shown here).

Charts with percentage of outliers (Figures 6 and 7) demonstrate the effect for different ensemble sizes (10, 20, 30, 40 and 50 members, for surface, 850 hPa and 500 hPa and both experiments). The presented scores are for Temperature, but very similar results can be observed for all other verified parameters like Geopotential, Wind Speed, Relative Humidity and MSLP.

The scientific report from the stay will be available on RC LACE web pages (www.rclace.eu).

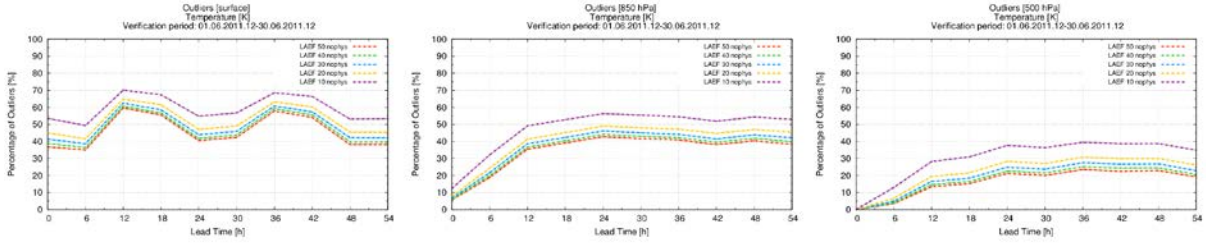

Figure 6: Percentage of outliers for temperature at the surface, 850hPa and 500hPa for different sizes of LAEF ensemble; experiments without multiphysics.

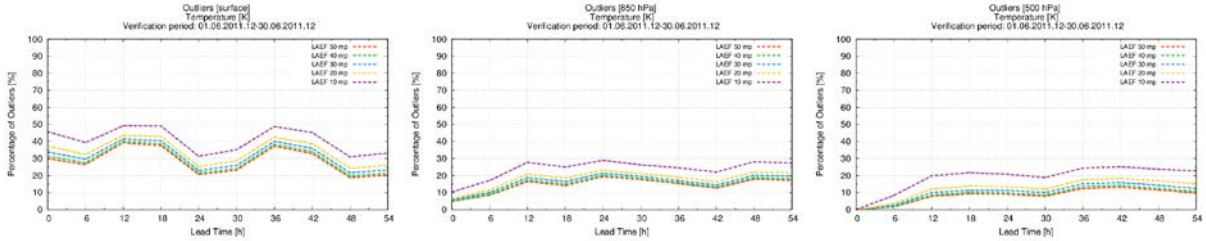

Figure 7: Percentage of outliers for temperature at the surface, 850hPa and 500hPa for different sizes of LAEF ensemble experiments with multiphysics.

Verification of new ALADIN-LAEF setup

New ALADIN-LAEF system on new domain with 10.9km resolution contains breeding + ensemble surface assimilation with perturbed observations + upper air blending; multiphysics retuning. 2-months verification scores for this experiment are confronted with the "old" LAEF system and pure ECMWF downscaling for the period from June 15th till August 15th 2011. Following conclusions has been drawn:

- New tuning of multiphysics is rather aggressive for some members (Figure 3).
- There is a bigger initial spin up for new ALADIN-LAEF system due to the perturbed observations - that was expected (Figure 4).
- Generally the scores are clearly better for new ALADIN-LAEF system in comparison with the old one and with the pure downscaling of ECMWF EPS forecast (Figure 5).

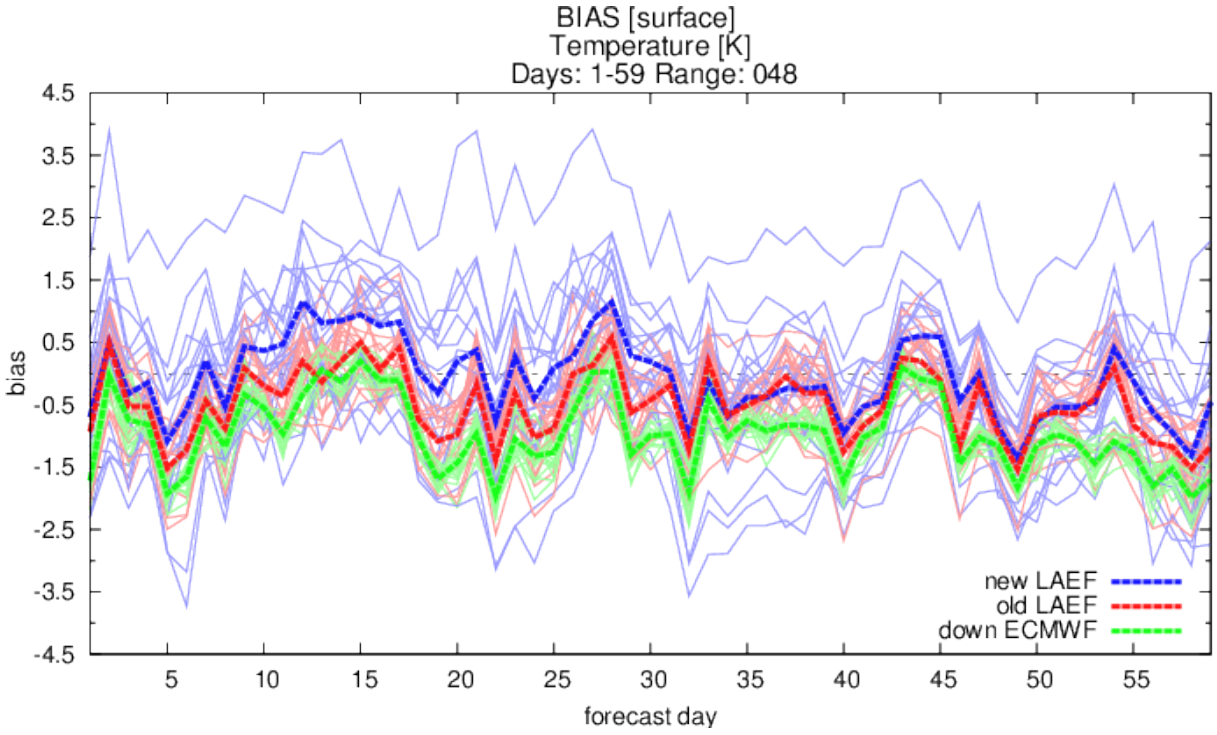

Figure 8: The day-by-day evolution of BIAS of 2m temperature for new LAEF setup (blue curves), old LAEF setup (red curves) and downscaled ECMWF EPS (green curves) for all LAEF ensemble members. The thick dashed lines are for EPS mean.

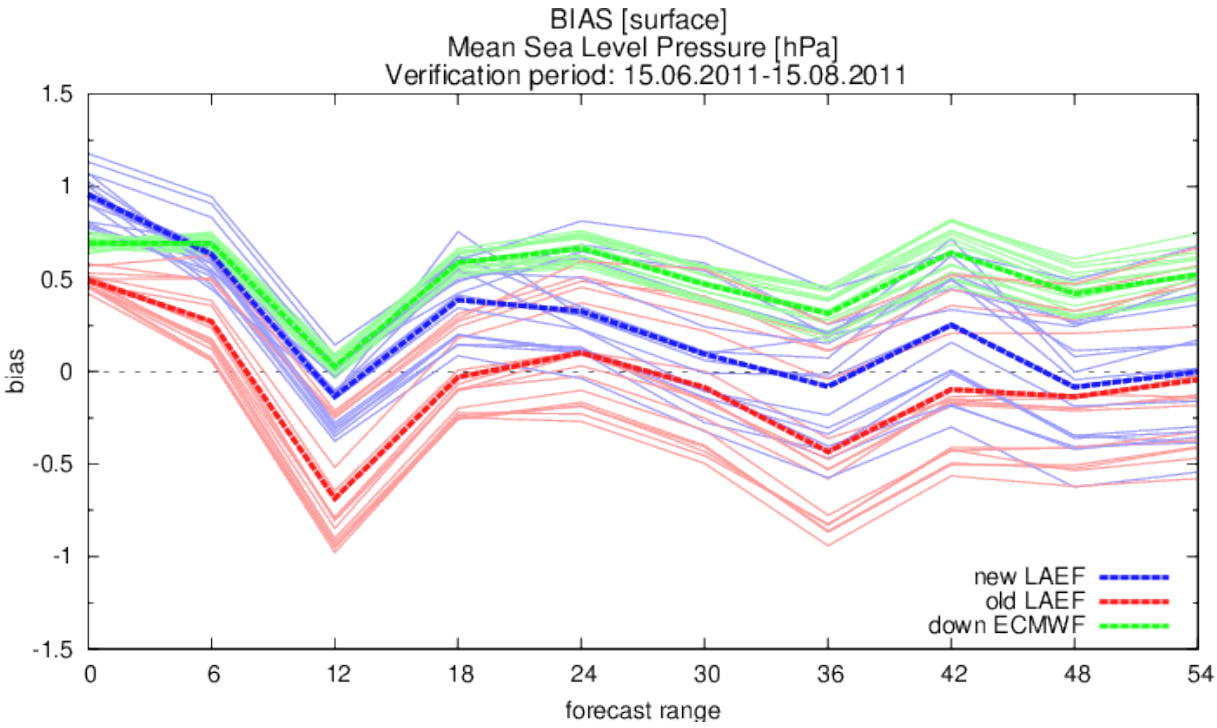

Figure 9: BIAS of mean sea level pressure for three described ALADIN-LAEF setups, averaged over 2 months period, for all forecast range.

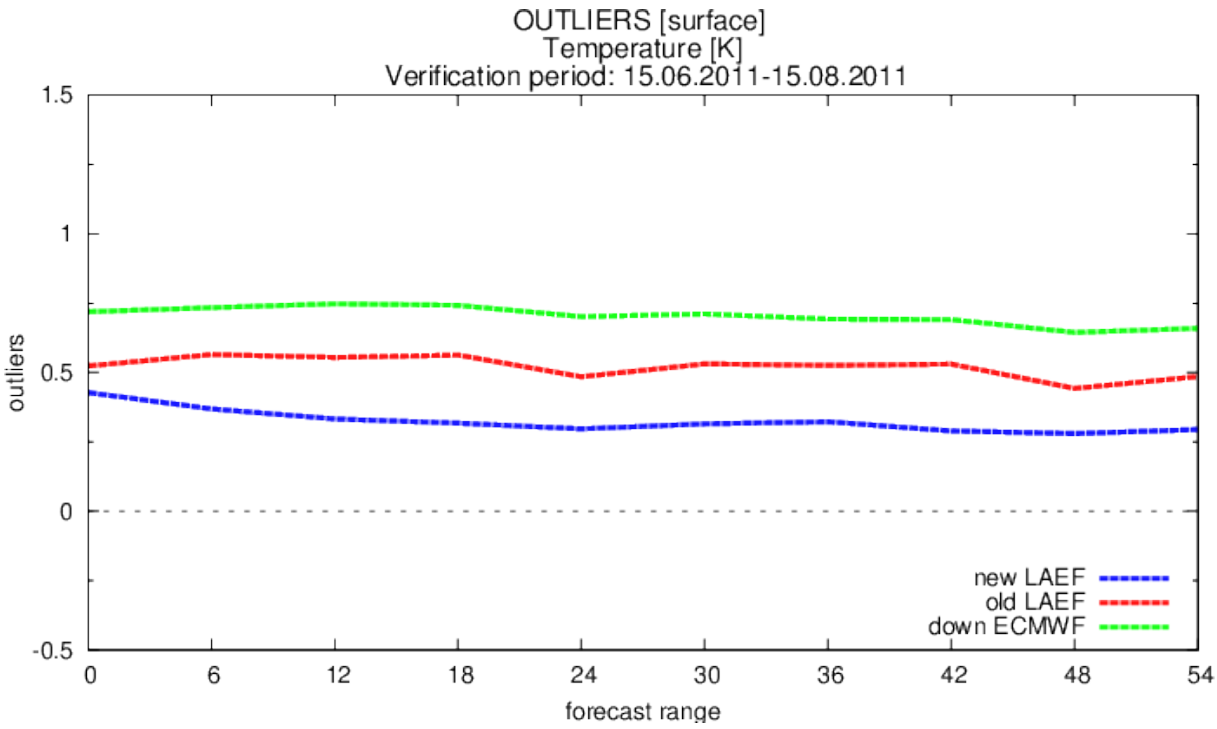

Figure 10: Number of outliers for new and old LAEF setup and for downscaled ECMWF EPS.

References

Belluš, M.: Time Consistent versus Space Consistent coupling and the revision of the Ensemble of surface Data Assimilations by CANARI in ALADIN/LAEF.
Report on stay at ZAMG, Vienna, Austria, 2013. Available on www.rclace.eu.

Belluš, M.: New LAEF Verification Package development and LAEF ensemble size sensitivity experiments.
Report on stay at ZAMG, Vienna, Austria, 2013. Soon available on www.rclace.eu.

Vivoda, J. and Smolíková, P.: Finite elements used in the vertical discretization of the fully compressible forecast model ALADIN-NH.
ALADIN - HIRLAM Newsletter no. 1, September 2013, pp 31-46

Vivoda, J: VFE discretisation of NH dynamics of AAA system.
Report from RC LACE stay, Prague, 2013. Soon available on www.rclace.eu.

Wittmann, Ch.: Near Maximum Overlap Version for ACNPART.
RC LACE report available on www.rclace.eu, 2009

ALADIN in Slovenia: highlights of 2013

Benedikt Strajnar, Neva Pristov, Jure Cedilnik, Jure Jerman

1 New HPC at Slovenian Environmental Agency

Slovenian Environmental Agency has been running a large investment project, with the title "Upgrade of the system for monitoring and analysis of the water environment", partially financed by EU cohesion found. One of the major deliverable is also the renewal of the IT center and upgrade of high performance computing facilities.

The public procurement was issued at the end of 2012. The new SGI ICE X HPC system was delivered at the end of April 2013. The main hardware characteristics are:

- 62 compute nodes (2 processors, 8 cores Intel Sandy Bridge architecture, 32 GB of memory per node),
- 3 service nodes (login, system management),
- two Infiniband FDR (56 Gb/s) interconnect,
- two NFS storage servers in HA mode with 120 TB of storage space,
- water cooled cabinets.

The queuing system is PBSPro. Unique feature of the system are "green queues" where non-urgent computing jobs can be performed at the price of slightly longer execution but substantively smaller power consumption.

The system will allow us to further increase the horizontal and vertical resolution of operational ALADIN model. Furthermore it will be possible to perform research at the horizontal resolution around 2 km. It will be used also for ocean, pollution dispersion and drought modeling.

2 Data assimilation of Mode-S aircraft observations

Data collection

Since May 2011, Mode-S meteorological data, collected by a traffic-control radar located at Ljubljana Airport, Slovenia, have been provided to the Slovenian meteorological office (ARSO) by Slovenia Control, Ltd. The data includes direct wind and temperature information contained in Mode-S register BDS 4.4 (Meteorological Routine Air Report). Based on data analysis, roughly 5 % of all aircraft over Slovenian airspace report meteorological information.

Preprocessing

The preprocessing of Mode-S is based on a comparison with operational ALADIN forecasts on a 2-year period. A white list of aircraft with good data was generated. Based on the phase of flight, a smoothing algorithm is applied to raw data with temporal resolution of 4 seconds. The smoothing period is 12 seconds (4 consecutive measurements) for ascents/descents and 1 minute for en-route phase of flights. The data is coded to text format (obsoul) and used experimentally for data assimilation.

Data assimilation experiments

The impact of Mode-S observations were also evaluated within the 3-hourly ALADIN data assimilation cycle. The main conventional upper-air information for ALADIN are AMDAR observations which are rarely available in the lower atmosphere near Ljubljana airport. With the usage of Mode-S observations, the spatial coverage was therefore locally significantly improved. The preprocessed Mode-S observations were assimilated together with AMDAR data. The assimilation experiments were carried out over 3-month period. Based on the verification against Mode-S observations in the 270 km radius around Ljubljana airport, there was a systematically positive impact on wind forecasts till around T+3 hours of the forecast. For temperature forecasts, it could be observed that assimilated Mode-S decrease systematic errors (bias) in the first hours of forecast. Mode-S data assimilation systematically improves temperature analysis and forecasts up to T+4 hours in the free atmosphere, but also up to T+12 hours near the surface. No significant degradations can be observed due to assimilated Mode-S. It can be concluded that collected data from Mode-S radar improves weather forecasts in nowcasting/short-range scales (see Fig. 1).

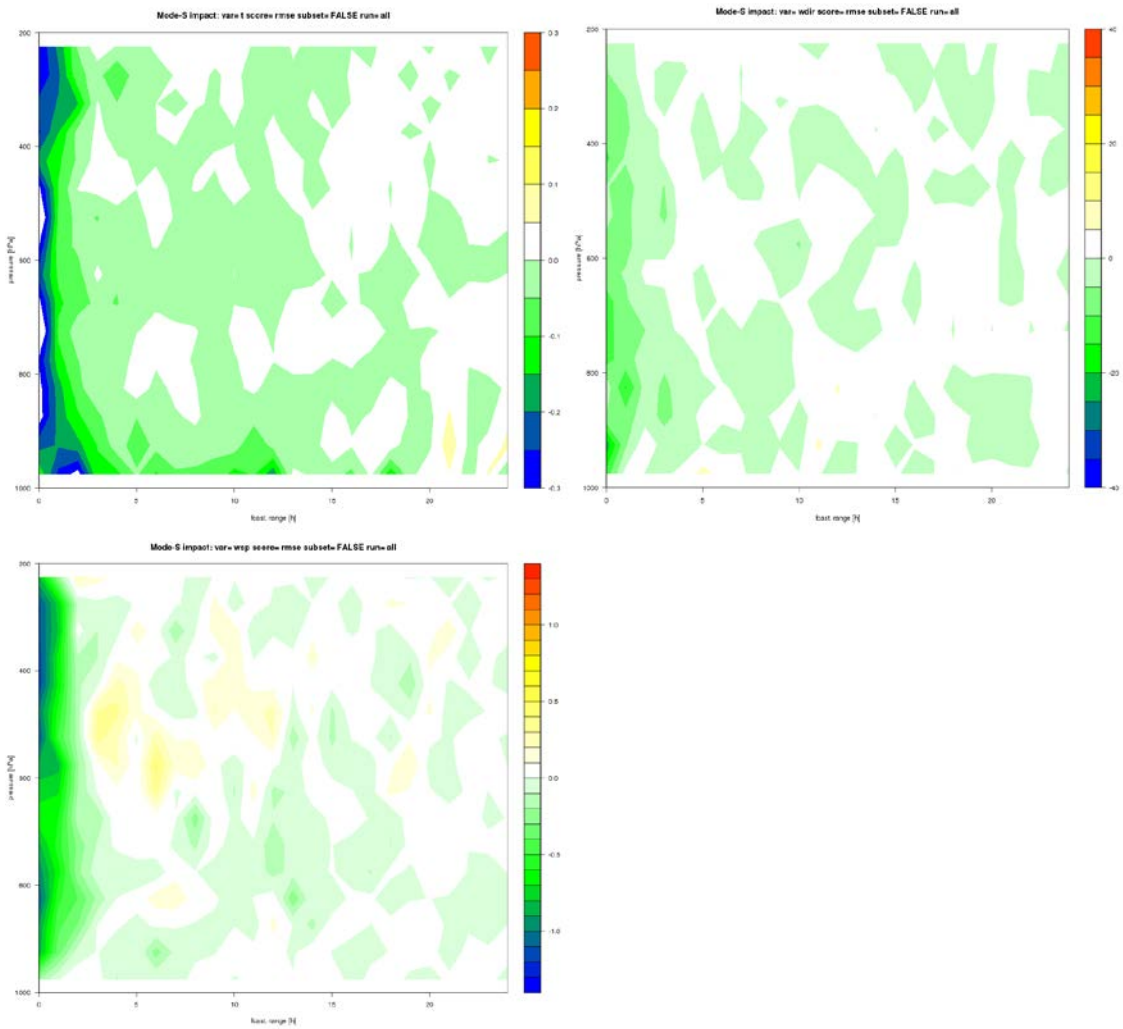

Figure 1: RMSE improvement (negative values) on short-range weather forecasts due to assimilated Mode-S winds and temperatures for temperature (upper left), wind speed (upper right) and wind direction (lower). Verification is against Mode-S observations.

AROME prototype over Tunisia

Ben Romdhane R.

1 Introduction

The AROME prototype of Tunisia has been created and installed on the server of Météo- France since December 2012.

2 Layout

Characteristics of the domain

The characteristics of the working domain and cycle are described in the following table.

Table 1: Characteristics of AROME-Tunisia prototype

Model version	CY37_t1.op1.07
Resolution	2.5 km
Levels	60
Domain	AROME-Tunisia
Number of points	400*550
Coupling files	ARPEGE
Starting time	00 UTC
Cycle interval	3 hours

Case study: October 30th 2011

Some case studies were made to see the behaviour of AROME model in convective situations and to compare the results with those obtained by ALADIN-Tunisia operational and with observations.

During the situation of the October 30th 2011, ALADIN provides a cumulative rain over 24 hours not exceeding 60 mm in the north and center of Tunisia, however, AROME triggers a core of rain centered on the north-east of Tunisia, with an intense rainfall exceeding 120mm, which is closer to the observations, as described below in the figure 1.

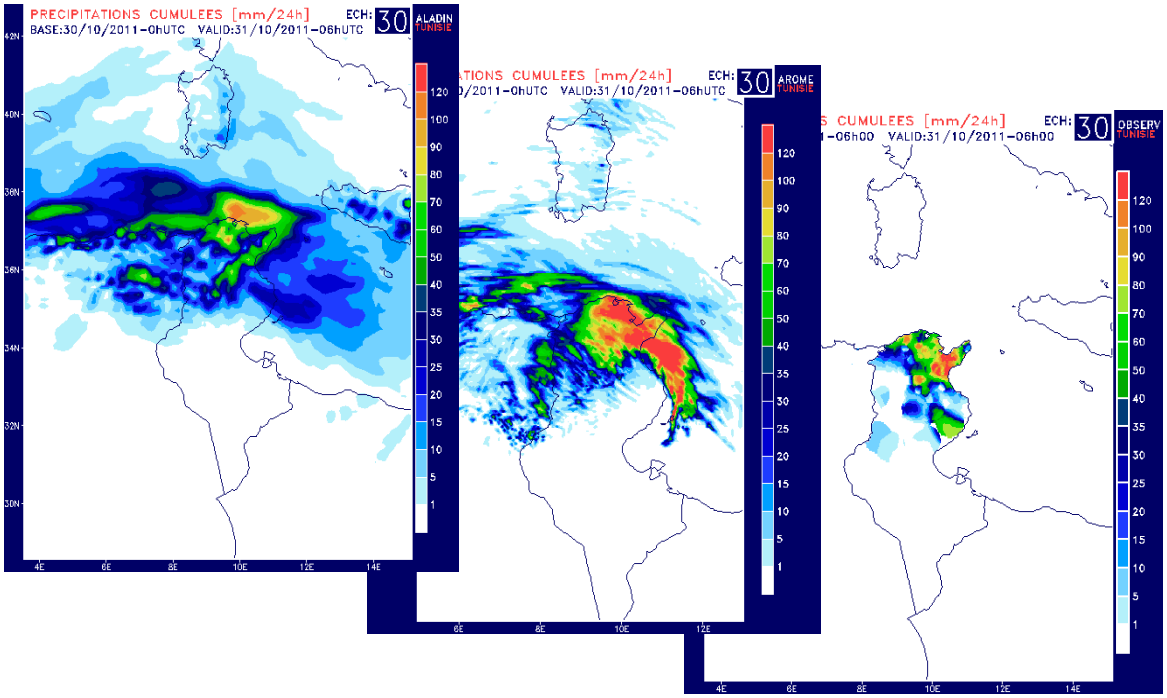

Figure 1: Study of the October 30th 2011 situation

List of events

Meetings

- 24th ALADIN Wk & HIRLAM ASM 2014 : 7-10 April 2014, Bucharest
- ALADIN LTM meeting : 8 April 2014, Bucharest
- HMG/CSSI meeting on 11 April 2014, Bucharest

- 11th PAC Meeting : Lisbon, 19 May 2014

- 2nd HAC/PAC meeting : Lisbon, 19 May 2014
- HAC meeting : Lisbon, 20 May 2014

- HIRLAM Council : Reading, 10 July 2014

- 36th EWGLAM & 21st SRNWP meetings : 29 September – 2 October 2014, Offenbach
- ALADIN LTM meeting : 30 September 2014, Offenbach

- ALADIN GA in Alger (week 48 or 49)
- HIRLAM Council (back-to-back with ALADIN GA or besides ECMWF Council, week 49)

Working Weeks

- ALARO-1 WW in Vienna, 12-14 May 2014
- HARP meeting in Brussels, 24-29 March
- HIRLAM EPS working week 19-23 May, Barcelona
- HIRLAM Radar working meeting, either in 10-14 or 24-28 March, Norrkoping
- HARMONIE system working week, date TBD, Helsinki
- HARMONIE System working week in Bratislava, dates to be defined
- ECMWF workshop on scalability and HPC issues, 14-15 April Reading
- HARMONIE training course for newcomers, 15-19 September, presumably Norrkoping.
- ALADIN-HIRLAM Forecasters' meeting in Ankara, date TBD
- HIRLAM EPS working week in November? Dates and place TBD
- DA/use of obs working week in fall (October?)
- ALARO baseline validation in Brussels, 2nd semester, date TBD
- HIRLAM Radiation working week, date and place TBD
- HIRLAM Surface working week, date and place TBD.
- HIRLAM Dynamics working meeting in Valencia, date TBD

For up-to-date information about the events please visit the consortium websites at:
http://www.cnrm.meteo.fr/aladin
http://hirlam.org